THE EFFECT OF TURBULENCE ON THE DRAG OF AIRSHIP MODELS

by

Hilda M. Lyon,

M.A. of the University of Cambridge, England.

Submitted in partial fulfillment of the requirements
for the Degree of
Master of Science
from the

Massachusetts Institute of Technology
1932

Department of Aeronautical Engineering.
January 20. 1932.

Professor in charge of research

Chairman of Departmental
Committee on Graduate Students

Head of Course.

January 20, 1932.

Professor Allyne L. Merrill,
Secretary to the Faculty,
Massachusetts Institute of Technology,
Cambridge, Massachusetts.

Dear Sir,

In compliance with the requirements for the degree of Master of Science from the Massachusetts Institute of Technology, I submit herewith a thesis entitled 'The Effect of Turbulence on the Drag of Airship Models'.

Respectfully yours,

Hilda M. Lyon.

Acknowledgement

The experiments described in this thesis were carried out under the direction of Professor R. H. Smith of the Department of Aeronautical Engineering. The author is indebted to Professor Smith for his advice and co-operation, and to Messrs. Whipple and Sauerwein for their assistance in the design and erection of the apparatus.

The Effect of Turbulence on the Drag of Airship Models

Contents

Diagrams.

Diagrams (continued)

References.

1. N.A.C.A. Technical Note 264, Figs. 3,4,5.

2. Dryden and Kuethe, N.A.C.A. Reports 342,392.

3. Relf and Lavender, R.M. 597.

4. B.M.Jones. R.M. 1199 and R.Ae.S.Journal,May 1929,p.363

5. H.Roxbee Cox. R.Ae.S.Journal, Sept.1929,p.800. Appendix IV.

6. R.Jones and Bell. R.M.1168.

7. B.N.Wallis. Aircraft Engineering, January 1930,Vol.II p. 7.

8. Pannell and R.Jones. R.M. 607.

9. Relf and Simmons. R.M. 917.

10. Ower and Hutton. R.M. 1271.

11. Richmond. Engineering. Vol. 130. p. 341, 1930.

12. Blasius. Z.M.P. 1908, Band 56, Heft 1.

13. Wieselsberger. E.A.V.G. Lieferung 1, S.120-124.

14. Prandtl. E.A.V.G. Lieferung 3.

15. Schiller and Hermann. N.A.C.A. Tech Note 600 translated from Ingenieur-Archiv Sept. 1930.

16. R. Jones and Bell. R.M. 1169.

17. Simmons. R.M. 1234.

18. Upson. S.A.E. Trans. Vol.21, 1926,Part 1,p.615,Fig.7

19. Zahm, Smith and Louden. N.A.C.A. Report 291, Table III

20. Fage. R.M. 1231

21. Fage and Falkner. R.M.1315,Proc.Roy.Soc.,A.Vol.129, 1930.

22. Simmons. R.M. 1268.

Abbreviations.

N.A.C.A.	National Advisory Committee for Aeronautics, U.S.A.
N.P.L.	National Physical Laboratory, Teddington, England.
R.M.	Reports and Memoranda of the Aeronautical Research Committee, Great Britain
R.Ae.S.	Royal Aeronautical Society, Great Britain
Z.M.P.	Zeitschrift für Mathematik und Physik.
E.A.V.G.	Ergebnisse der Aerodynamischen Versuchsanstalt zu Göttingen
S.A.E.	Society of Automotive Engineers, U.S.A.

I. Introduction

The degree of initial turbulence in the air stream of a wind tunnel has an important effect on the results obtained from measurements of the resistance of airship models. This effect was clearly demonstrated by the international tests on two N.P.L. models, which showed a wide range of values for the resistance of the same model when tested in different tunnels at the same Reynolds number. A summary of the results of the tests in the American tunnels covers the whole range. (Reference 1). The highest values for the resistance coefficient, obtained in the tunnels with the most turbulent flow, were found to be approximately double the lowest values, obtained in the tunnels with a relatively smooth or non-turbulent flow, for a Reynolds number of 10^6-$4x10^6$. In some later experiments at the Bureau of Standards it was proved conclusively that such discrepancies were due to varying degrees of initial turbulence. (Reference 2). Experiments at the National Physical Laboratory showed that similar results could be obtained by placing a wire mesh screen inside the tunnel at various distances from the model. (Reference 3). The effect of turbulence on the shape of the curve showing the variation of drag coefficient with change of Reynolds number was explained

by Prof. B. M. Jones, in a paper before the Royal Aeronautical Society, by comparison with the behavior of the skin frictional coefficient for a flat plate. (Reference 4). For most streamline bodies the drag due to normal pressure on the surface is small compared with that due to tangential forces or skin friction. Measurements of the skin friction on a flat plate show that, for values of Reynolds number ($R=VL/\nu$ where L is the length of the plate) below about 10^5, the flow in the boundary layer is wholly laminar and the drag coefficient decreases with increasing Reynolds number. At some critical value ($Ro=VL/\nu$) the flow becomes turbulent at the rear end of the plate and the transition point between laminar and turbulent flow moves forward with increasing Reynolds number until practically the whole layer is turbulent. The value of Ro depends on the initial turbulence in the tunnel and on the shape of the leading edge. The distance 'x' of the transition point from the leading edge is given by $Vx/\nu = R_o$, or $x/L = R_o/R$. When the Reynolds number R is sufficiently large the laminar part of the boundary layer can be neglected. During the transition stage the drag coefficient increases with the Reynolds number and then decreases again more slowly when the flow in the boundary layer is almost wholly turbulent. For airship models the variation of the drag coefficient expressed

in terms of surface area shows the same tendency. Unfortunately the values of Reynolds number used in most wind tunnels fall within the critical range in which the change from laminar to turbulent flow occurs. Within this range the flow in the boundary layer is sensitive to extraneous disturbances in the air stream. For the Reynolds number appropriate to the full scale airship, it is concluded that the flow is, in effect, turbulent throughout the whole boundary layer, the laminar flow at the extreme nose covering too small an area to have an appreciable influence on the drag. The critical Reynolds number R_o is greater for a streamline body than for a flat plate and varies with the initial turbulence in the tunnel and also with the shape of the body. Thus, in comparative tests on two shapes at the same Reynolds number and in the same wind tunnel, it may happen that for one shape the transition point is much further forward than for the other, and the drag coefficient correspondingly higher. On the full scale airship, where the flow is turbulent for both shapes, this apparent difference in drag coefficient may be expected to disappear. Thus, for comparing the relative merits of two shapes, wind tunnel tests within the transition range may be most misleading.

In the experiments described in this report an attempt has been made to eliminate the effect of the shape on the position of the transition point by producing turbulent flow in the boundary layers of both models by the use of screens which increase the initial turbulence in the wind tunnel stream. The two models were deliberately chosen to give widely different drag coefficients when tested in a tunnel of comparatively small turbulence at a Reynolds number of about 2×10^6. The results show that the effect of increasing the initial turbulence is to decrease the difference between the drag coefficients of the two models until they finally become equal. It was expected that when the boundary layer became almost wholly turbulent the drag coefficient of either model at a given Reynolds number would tend towards a maximum value beyond which any further increase in extraneous turbulence would have no effect. The results of the experiments do not give any clear indication of the existence of such a maximum value, but the turbulence calibration curve for the higher values is not sufficiently reliable to allow of a definite conclusion on this point.

In the Bureau of Standards' Reports referred to above, (Reference 2), the quantity which determines the intensity of turbulence is defined as the 'ratio of the

square root of the mean square of the deviations of the speed from its mean value to the mean value'. This definition assumes that the amplitude of the local speed fluctuations is the determining factor, and makes no allowance for the effect of frequency. In an attempt to show the relative effects of amplitude and frequency, three screens were used in the experiments and were designed to produce eddies whose frequencies were inversely proportional to the linear dimensions of the mesh. The results show that the frequency of the disturbances is much less important in its effect on the drag of an airship model than the amplitude.

II. The design of models and apparatus

1. Models.

The two models used in the experiments were designed to show the effect of varying the shape rather than the fineness ratio. They were therefore made of the same length and maximum diameter with a fineness ratio of 5:1, (length L = 35 ins., maximum diameter D = 7 ins.) (Fig. 1.). The shape of the first one, model A, was originally developed in the course of the design of R.101 by a method described by H. Roxbee Cox (Reference 5). Apart from the difference in fineness ratio, it is the same as Shape 5, (Reference 5) which differs only slightly from the shape

3a of Reference 6, which was finally adopted for R.101, and closely resembles R.100 (Reference 7) and U.721 (Reference 8), all three of which gave approximately the same minimum drag coefficient, the lowest of any shapes tested in the N.P.L. tunnels. The analytical method used for the development of the equation of the generating curve differs somewhat from the method referred to above (Reference 5). In terms of the non-dimensional coordinates $s = x/L$ and $z = y/D$, where x is the distance from the nose of the model and y the radius of the circumscribing circle (Fig.1), the equation to the generating curve of an airship shape may be expressed in the form:-

$$z^2 = as + bs^2 + cs^3 + \text{----} + ks^n + \text{----}$$

which satisfies the condition that $z = 0$ when $s = 0$. Using the first four or five terms in this series, a wide variation of shapes can be obtained. The coefficients can be chosen to satisfy the necessary conditions that $z=0$ when $s=1$, and $z=.5$ when $dz/ds = 0$, and any other required conditions such as:- $dz/ds = 0$ when $s = s_m$ and $\int_0^1 z^2.ds = k_b/4$, where s_m is the desired position of the maximum diameter and k_b is the block coefficient (the ratio of the volume to the volume of the circumscribing cylinder.) The equation for model A expressed in this

form is:-

$$z^2 = 1.23935\ (s - s^2 - s^3 + s^4).$$

The position of the maximum diameter is given by s_m = .3904, and the block coefficient is k_b = .5785.

The same type of equation, with five terms, was used for model B, with the conditions that s_m = .4, k_b = .7, and z = .4 when s = .1, the latter condition being chosen to ensure a bluff nose. These conditions give:-

$$z^2 = 2.3390s - 9.0020s^2 + 17.8238s^3 - 17.6885s^4 + 6.5279s^5.$$

The corresponding values of s and z for both shapes are given in Table 1, and also the values of x and y in inches for the models actually used, together with other relevant data.

2. Apparatus.

The experiments were carried out at the Massachusetts Institute of Technology in the large tunnel, which has a closed throat of circular cross section, 7.5 feet in diameter, and open return flow through the room. The maximum speed used was 60 mph. For the drag measurements the model was supported by two vertical wires attached to the ceiling of the room and was free to move along the axis of the tunnel. (Fig. 2). The longitudinal displacement for various wind speeds was measured outside the tunnel by sighting a line on the model through a small telescope

mounted on a graduated scale. One of the supporting wires was attached directly to the model at a point 16 ins. from the nose, about 2 ins. behind the maximum diameter. The rear wire was clamped in a slot in a sting, 19 ins. long and 1/4 inch in diameter, attached to the tail of the model, and passed through the floor of the tunnel to a stability weight suspended below. To allow the wires to pass through, holes were cut in the tunnel and covered with adjustable brass plates. The wires passed through narrow slits, about 8 ins. long, in the brass plates, with sufficient clearance to allow them to move freely during the displacement of the model in the wind. To prevent lateral movement, a bead fitted over the sting was attached by horizontal wires with turnbuckles to the sides of the tunnel and adjusted to allow free longitudinal movement of the sting. The forward wire passed through a slit in a narrow brass plate (1/2 inch wide and 9 ins. long) which was supported by means of four horizontal wires, fitted with turnbuckles, at a distance of 8 ins. above the upper surface of the model. Careful adjustment of all turnbuckles was required to ensure free longitudinal movement. All readings of displacements were repeated several times, the model being first disturbed by moving the stability weight and then allowed to return

to the equilibrium position. Once the zero reading had been satisfactorily determined no difficulty was encountered in repeating the readings at the various wind speeds. The combined drag of the model and the moving parts of the apparatus was calculated from the formula,

$$\text{Drag} = Wh/\ell$$

where W = the weight of the model and moving parts,

h = the displacement of the model,

ℓ = the length of the supporting wires.

The calibration was checked by means of a weight attached to the end of the sting by a horizontal wire passing over a pulley. An attempt was made to measure the required correction for the wire drag by duplicating the supporting wires, but it was found that the wire drag in the worst case was approximately double the drag of the model alone and the correction was considered too large for reasonable accuracy even for comparative purposes. Metal shields were therefore made to cover practically the whole of the rear wire inside the tunnel and the part of the forward wire above the brass plate. The remaining parts of the wires inside the tunnel were then duplicated and the parts outside either shielded or duplicated. The correction for wire drag was estimated from the difference between the measured drag with the double wires and that

with the single wires. The addition of the shields reduced the wire drag correction to about 7-14% of the model drag. The measured values of the wire drag were found to be from 2 to 10% less than the calculated values. No correction was made for the drag of the sting as it had been found to be negligible in previous experiments of the same type in other tunnels.

The models had a slight lateral oscillation at 50 and 60 mph., but no oscillation was perceptible at the lower speeds and no longitudinal oscillation at any speed.

3. Screens.

Turbulent flow in the boundary layer of an airship model can be produced either by disturbing the air in the tunnel by the introduction of screens, or by placing a thread or wire round the nose of the model. (References 3 and 10). The first method was chosen for these experiments so that it would be possible to compare the drag coefficients of the two models when placed in the same turbulent stream. Each of the three screens consisted of horizontal and vertical rods or wires of circular cross section and was placed at various distances from the nose of the model. (Fig. 2). In designing the screens the ratio of the spacing between the wires to the wire diameter was kept constant and the following dimensions

were used:-

Screen 1. 1/4 inch rods with 4 inch spacing.

Screen 2. 1/8 " " " 2 " "

Screen 3. 1/16 inch wires with 1 inch spacing.

The first two screens were made from straight steel rods fastened to a circular ring, but the third was constructed of manufactured wire netting, in which each wire was bent in a series of waves producing an elliptic instead of a circular cross section in the wind direction. This seems to have affected the pressure distribution behind screen 3 as compared with that behind screens 1 and 2 but not the amplitude or the frequency of the disturbances so far as can be determined from the experiments. Measurements of the frequency of eddies behind circular cylinders have shown that there is a close connection between the variation of the eddy frequency and that of the drag coefficient with changing Reynolds number. (Reference 9).

The diameters of the wires in the screens were chosen to be within the range of Reynolds number (8×10^2-2×10^4) for which the frequency of the eddies is approximately proportional to the wind speed and inversely proportional to the wire diameter. It has been assumed that this relationship between eddy frequency and wire diameter is not affected by the interference between adjacent wires

provided that the distance between the wires is proportional to the wire diameter. The amplitude of the disturbances was varied by moving the screen relative to the model.

III. Tests on a sphere for the measurement of turbulence.

Measurements of the drag of a sphere were used to give an indication of the intensity of the turbulence in the tunnel in accordance with the definition quoted above in paragraph I (see Reference 2). The diameter of the sphere (7.8 inches) was chosen so that the range of speeds which could be used (10-60 mph.) would cover the critical range for which the drag coefficient of a sphere falls rapidly with increasing Reynolds number. The critical Reynolds number at which this change occurs decreases with increasing turbulence and the curve in Fig. 4 shows the percentage turbulence corresponding to the Reynolds number for which the drag coefficient of the sphere is equal to .3. This curve was reproduced from Fig. 9, of N.A.C.A. Report 392 (Reference 2) and was derived from measurements of sphere drag combined with measurements of turbulence with a hot-wire anemometer at the Bureau of Standards.

The sphere drag was measured in the same way as the model drag by observing the displacement through a telescope. A sting, 1/2 inch in diameter, was attached behind the sphere and supported by two wires from the top of the tunnel, while a third wire from the sting passed through the slit in the floor to the stability weight. (Fig. 3). Lateral motion of the sphere was prevented by two beads fitted over the sting and attached by horizontal wires with turnbuckles to the walls of the tunnel. For the zero reading careful adjustment of the turnbuckles was required to ensure free longitudinal movement, but at speeds above 35 mph a certain amount of friction between the beads and the sting was found to be useful in damping out the longitudinal oscillations of the sphere. After the first reading at any particular speed the sphere was displaced by moving the stability weight and a second reading was taken as soon as the oscillations had ceased. The process was repeated several times and if the reading could not be repeated the amount of damping was reduced and a second series of readings taken. In some cases for speeds within the critical region the readings were persistently erratic and an average value had to be used.

The drag of the wires and sting was measured with the sphere supported separately in the correct relative

position. The measured drag was found to be from 0 to 10% less than the calculated drag for the wires alone and varied from 10% of the drag of the sphere at low speeds to 40% at high speeds, being about 20% at the critical Reynolds number corresponding to a drag coefficient of .3.

For any one position of the screen the distance between the sphere and the screen varied with the displacement at different speeds. This variation was small but was allowed for by plotting the results for each speed against the distance of the centre of the sphere from the screen after displacement. (Figs. 5, 7, 9) The curves were faired when necessary, and the method thus eliminated doubtful readings and gave more consistent results. From these curves were derived the curves of Figures 6, 8, 10 showing the variation of the drag coefficient with Reynolds number for each screen at various distances from the sphere. The values of Reynolds number for which k_d = .3 were taken from these curves and plotted in Figure 11 against the distance between the screen and the centre of the sphere. The percentage turbulence for various screen positions, shown in Figure 12, could then be found by combining Figures 4 and 11. Unfortunately the critical values of Reynolds number obtained behind the screens were in many cases beyond the range of the Bureau of

Standards' tests on which Figure 4 was based, and it was necessary to extrapolate the curve.

The results show that, at a given distance from the sphere, the screen with the largest size of wire and mesh had the greatest effect in producing turbulence, but a wider range of turbulence could be obtained by halving the distance between the screen and the sphere than by doubling the size of the wire and mesh. It is important to note that the presence of even the finest screen had a considerable effect on the turbulence with the sphere 11 feet away. None of the screens had any appreciable effect on the drag of the airship models when placed at a distance of more than 8 feet from the maximum diameter of the model.

IV. Measurement of wind speed and pressure gradient.

For recording the speed a static tube was placed in the tunnel in front of the screen and connected to an Ellison gauge, the other end of which was open to the atmosphere in the room. The gauge was calibrated by means of a pitot tube placed on the centre line of the tunnel in the working section and connected to an N.A.C.A. manometer. Re-calibration was necessary for each screen and was carried out with the screen in position 1 (Fig.2)

In calculating the speed from the dynamic head, standard conditions were used, as the effect of varying atmospheric conditions on the Reynolds number was considered to be unimportant.

For measuring the pressure gradient a static tube fixed in the tunnel wall behind the working section was used as datum, and the pitot tube used for the speed calibrations was moved along the tunnel in line with the centre of one of the square meshes, in the case of screen 1, and for screens 2 and 3 in line with the centre line of the model. The static pressure difference between the two tubes was read in inches of alcohol on the N.A. C.A. manometer for wind speeds of 20,30,40,50, and 60 mph. The results were divided by the dynamic head, $q = \rho V^2/2$, in inches of alcohol, and the average values for the four higher speeds were used. (Fig. 14 etc.) The pressure behind the first screen was measured without the metal shields for the supporting wires, and the values of p/q plotted in Fig. 14 show the effect of the screen alone on the pressure variation along the tunnel. In the tunnel without any screen and for positions (1) and (4) of the second and third screens, the pressure was measured both with and without the wind shields. From these results the pressure variation for the shields

alone was deduced (Fig. 13) and superimposed on Fig. 14 to give the pressure variation behind the first screen with the shields in place, as shown in Figure 15. The values of p/q behind screens 2 and 3 and with no screen in the tunnel are shown in Figures 16 and 17 with the wind shields in the tunnel.

The pressure gradient for the second screen was not intermediate between those for the first and third screens. This may have been due to the different method of construction used for the third screen.

Immediately behind the screen there was a local variation in the pressure across the tunnel due to the effect of the wires. This was not investigated in detail but several readings were taken with the pitot tube in different positions to estimate the range of variation. The two curves in Fig. 16 for the fourth screen position illustrate the maximum difference in pressure found for any two positions of the pitot. The effect on the drag of using the pressure at the centre of the tunnel instead of at the centre line of the model would be to increase the estimated model drag by 2.6 per cent. There was also a perceptible transverse pressure gradient below the forward wind shield, giving a maximum pressure difference within the region occupied by the model of .04q. The

possible error due to this cause has been estimated to be less than 2% of the model drag. The interference of the forward wind shield on the flow near the model introduced an undesirable effect which partly counterbalanced the gain in accuracy due to the elimination of the forward wire drag, and it is thought that more accurate results might have been obtained by the use of the rear wind shield only.

As the pressure gradient along the tunnel was not constant it was necessary to integrate the longitudinal component of the static pressure over the surface of the model in its displaced position to find the required correction to the measured drag. In accordance with the conventional approximate method this correction was assumed to be:-

$$F - F_0 = \delta F = \pi q \int_{x=0}^{x=L} (p/q)\,d(y^2).$$

where F is the measured drag of the model and F_0 the corrected drag. Owing to the displacement, the position of the model in the tunnel was different at different speeds. The integration was carried out for each case for wind speeds of 20,40 and 60 mph and values were interpolated for 30 and 50 mph assuming that $\delta F/q$ varied linearly with the displacement. The maximum corrections were within ∓ 25% of the model drag. (see Tables 2-7)

V. Results of the experiments on airship models.

If f be the intensity of skin friction tangential to the surface of the model at a point (x,y), then the drag due to skin friction is given by:

$$F = \int_{x=0}^{x=L} f.2\pi y \ .dx = Sf_o.$$

where f_o is the mean intensity of skin friction and

$S = \int_{x=0}^{x=L} 2\pi y.dx$, the 'effective' surface area.

The results of the drag measurements have been expressed in terms of the non-dimensional coefficient k_f, where

$$k_f = F/qs = f_o/q, \quad q = \rho V^2/2.$$

and F = the total model drag, including the part due to the integration of the normal pressure over the surface.

Tables 2-7 give a complete record of the measured displacements, the equivalent measured drag, the corrections for wire drag and pressure gradient, the model drag and the coefficient k_f for both models. The values of k_f have been plotted in Figs. 18, 19, 20 against log R where $R = VL/\nu$, the Reynolds number for the model. A few representative cases plotted in Fig. 21 on a logarithmic scale, in conjunction with the curves for a flat plate in laminar and turbulent flow, give a better idea of the variation of the model drag with turbulence and its relation to the full scale value. The model and full scale results for R.101 are also shown. The model values have

been taken from Reference 6, and the full scale result has been deduced from the fact that the speed predicted from the minimum model drag was in good agreement with the speed attained on the actual airship. (Reference 11)

The curve for laminar flow on a flat plate was first derived by Blasius (Reference 12) from the integration of Prandtl's boundary layer equations. The upper curve (1) for turbulent flow was developed empirically by Wieselsberger (Reference 13) and the lower one (2) by Prandtl by a combination of theoretical and experimental results. (Reference 14). A later modification of this curve (Reference 15) is in closer agreement with curve (1) at the higher values of Reynolds number. The third turbulent curve (3) shows the effect on the skin frictional coefficient of the increased speed over the surface of an airship. For the flat plate,

$$\int_0^L f.dx = k_f.\rho V^2.L., \text{ where, for curve (2),}$$

$$k_f = .0375(VL/\nu)^{-0.15}$$

Then $f = .0319\ \rho V^2(Vx/\nu)^{-0.15}$

For the airship it was assumed that

$$f = .0319\ \rho U^2(Ux/\nu)^{-0.15},$$

$$k_f = \frac{1}{Sq}\left(\int_o^L f.2\pi y.dx\right)$$

where x = the distance along the axis from the nose of the ship,

$$U = V\sqrt{1-p/q},$$

$$q = \rho V^2/2.$$

$$S = \int_0^L 2\pi y. \, .dx$$

The values of p/q were taken from the measurements on a model of R.101. (Reference 16).

The results for the two models behind screens show clearly the effect of turbulence on the drag coefficients for both shapes. With no screen, or with a screen placed 8 feet in front of the model, the curve for model A agrees well with the model tests on R.101 (Reference 6), showing a coefficient decreasing with increasing Reynolds number. The corresponding curve for model B has the form of a transition curve and rises steeply from R = 10^6 to a value of k_f at R = 1.6×10^6 about 50 per cent greater than the value for model A. As the screen is moved nearer to the model the two curves rise and change their shape and approach one another until they become practically coincident and roughly parallel to but above the flat plate curve for turbulent flow.

The variation of the coefficient k_f with the distance between the screen and the model is shown more clearly in Figs. 22 and 23 for the maximum wind speed of 60 mph. ($R=1.61 \times 10^6$). Figures 24 and 25 show the same variation plotted against percentage turbulence, as

derived from Fig. 12, assuming that the distance of the screen from the maximum diameter of the model is equivalent to the distance from the centre of the sphere, for the measurement of turbulence. It is probable that the intensity of the turbulence in the neighbourhood of the transition point is the true criterion. The upper parts of the curves in Figs. 24 and 25 are based on the extrapolated part of the curve of Fig. 4 and are therefore of doubtful value except for comparative purposes. There is no definite indication of a limiting maximum value beyond which increased turbulence has no effect on the drag coefficient. There is, however, a very definite lower limit, the value of k_f being constant over a considerable range of turbulence as indicated by the sphere. This does not mean that the boundary layer is wholly laminar for the lowest intensities of turbulence, since the lower limit exists not only for model A but also for model B for which the flow is apparently in a transition stage between laminar and turbulent conditions. The more probable explanation is that a certain minimum amplitude of disturbance is required to change the type of flow in the boundary layer.

It appears that the screen with the largest mesh has the greatest effect on the drag of a model for the same amplitude of disturbance, or 'percentage turbulence'.

This may be due to the effect of the frequency of the disturbance on the sphere rather than on the model. The scattering of the results (x) in Fig. 4 may be due to variations in the frequency of the eddies produced by the different honeycombs. The vertical distance between the upper and lower points is of the same order as the horizontal distance between the curves for screens 1 and 3 shown in Figs. 24 and 25. If the intensity of turbulence had been measured with a hot-wire anemometer it is just possible that the curves for the three screens might have been approximately coincident. In any case there is no doubt that the frequency of the disturbances is unimportant in comparison with the amplitude.

VI. Practical application of the results.

The relative merits of airship shapes are usually estimated in terms of the drag coefficiant k_d where,

$$K_d = \text{Drag}/qQ^{2/3},$$

$$Q = \text{volume} = \int_{x=o}^{x=L} \pi . y^2 . dx.$$

For both models A and B.

$$k_d/k_f = S/Q^{2/3} = 6.42.$$

and the ratio is approximately constant for all streamline bodies of the same fineness ratio, and varies as the cube root of the fineness ratio.

The results shown in Fig. 21 suggest that for the full scale Reynolds number k_f has the same value for both shapes.

With this assumption two ships of the same volume and the same fineness ratio will have the same drag. In considering the speed and required horsepower there is therefore nothing to choose between the two shapes. From the structural point of view the shape with the higher block coefficient has a definite advantage, as it provides a greater gas volume in the nose and tail to balance the concentrated weights of the mooring equipment and the fins, (Reference 11), thus relieving the static bending moments on the hull and reducing the structure weight. As the structure weight in modern rigid airships is about 65 per cent of the total lift, a saving of 10 per cent on the structure weight means an increase of nearly 20 per cent in the useful load and probably 65 per cent in the 'pay load'. When results of the full scale tests on the U. S. Naval airship 'Akron' are available for comparison with R.100 and R.101, a partial check on the validity of the above assumption may be obtained, as the block coefficient of the 'Akron' is considerably higher than that of the British ships.

VII. Further developments.

Measurements of pressure along one generator of each model will shortly be carried out without any screen in the tunnel, and with screen 2, probably in a position

intermediate between (3) and (4). The drag due to normal pressures can then be found, and subtracted from the total drag to give the drag due to skin friction alone. The distribution of normal pressure over the surface has also an indirect influence on the drag owing to its effect on the growth of the boundary layer and on the local intensity of skin friction. It is expected that model B will show a lower minimum pressure than model A, followed by a steeper upward pressure gradient which is probably responsible for the earlier change from laminar to turbulent flow indicated by the drag coefficient curves with no screen in the tunnel. No experimental evidence is at present available with regard to the effect of artificial turbulence on the pressure distribution on a streamline body.

The results of the drag measurements on the two airship models seem to show that a definite minimum value exists for the amplitude of the disturbances necessary to produce turbulent flow in a laminar boundary layer at a given Reynolds number. If it be assumed that the required amplitude is proportional to the thickness of the boundary layer, it will increase with the size of the model for the same Reynolds number. The effect on the drag coefficient of the same degree of turbulence above

the minimum value probably varies also with the size of the model. Tests on larger scale models of shapes A and B behind screen 2 in various positions should illustrate the nature of this variation and may provide on explanation for the discrepancies between the drag coefficients measured in the N.P.L. tunnels for the 80" and 40" models of R.101. (Reference 22).

No information is available as to the distribution of the intensity of skin friction along the generator of a streamline body. Owing to the effect of the double curvature of the surface and of the pressure gradient it may be entirely different from the distribution along a flat plate. There is therefore no reason why the skin frictional coefficient k_f for an airship model should follow the flat plate curve shown in Fig. 21. Full scale tests, and model tests carried out under turbulent conditions suggest that a similar curve exists for a streamline body. This curve probably lies above the flat plate curve and rises with decreasing fineness ratio, owing to the increasing curvature and pressure gradient. The turbulent curve (3) of Fig. 21 allows for the effect of the increased speed over the greater part of R.101 due to the reduction in pressure. This effect would increase with decreasing fineness ratio owing to the increase in

the value of (1-p/q) over a large part of the surface. (Reference 18). If k_f were constant for varying fineness ratio, k_d would vary as the cube root of the fineness ratio. Model results show that, when L/D is less than 4, the value of k_d increases with decreasing fineness ratio and that for a range of L/D between 4 and 7 there is little change in k_d. (References 1 and 19). This effect may be due to an increase in the drag due to the integration of the normal pressure over the surface and also, in part, to an increase in the skin frictional drag due to the tangential forces. It is hoped that the publication of model and full scale data obtained in connection with the design of the 'Akron' will throw further light on this problem.

Information as to the local intensity of skin friction can be obtained from measurements of velocity or total head within the boundary layer of an airship model. (References 20,21).

An examination of the velocity distribution in the boundary layer will also give some indication as to whether the flow produced by extraneous disturbances is similar to that produced by increasing the Reynolds number. Measurements of total head within the boundary layers of three airship models at the N.P.L. (References 10 and 22) show

the same type of distribution over a large part of the boundary layer which is naturally turbulent, but no measurements were taken with screens or with wires round the nose to show the effect of artificial turbulence on the distribution of total head.

Table I. Model Dimensions.

	Model A.			Model B.	
s	z	x	y	z	y
.01	.11077	0.350	0.775	.15003	1.050
.03	.18981	1.050	1.329	.25008	1.751
.05	.24235	1.750	1.696	.31076	2.175
.10	.33230	3.500	2.326	.40000	2.800
.15	.39303	5.250	2.751	.44722	3.131
.20	.43631	7.000	3.054	.47338	3.314
.25	.46676	8.750	3.267	.48773	3.414
.30	.48666	10.500	3.407	.49530	3.467
.35	.49742	12.250	3.482	.49893	3.493
.3904	.50000	13.664	3.500		
.40	.49985	14.000	3.499	.50000	3.500
.45	.49461	15.750	3.462	.49891	3.492
.50	.48206	17.500	3.374	.49537	3.468
.55	.46255	19.250	3.238	.48851	3.420
.60	.43631	21.000	3.054	.47721	3.340
.65	.40352	22.750	2.825	.46010	3.221
.70	.36433	24.500	2.550	.43579	3.051
.75	.31883	26.250	2.232	.40284	2.820
.80	.26718	28.000	1.870	.35976	2.518
.85	.20937	29.750	1.466	.30506	2.135
.90	.14558	31.500	1.019	.23688	1.658
.95	.07575	33.250	0.530	.15172	1.062
.97	.04617	33.950	0.323	.11041	0.773
.99	.01574	34.650	0.110	.05857	0.410
1.00	.00000	35.000	0.000	.00000	0.000

	A	B	
Volume.	.451	.546	ft^3
'Effective' surface Area.	3.78	4.28	ft^2
$(\text{Volume})^{2/3}$	.588	.668	ft^2
Block coefficient.	.5785	.7000	
Distance of maximum diameter from nose.	13.664	14.000	ins.
Distance of centre of buoyancy from nose.	15.001	15.672	ins.

Table 2. Results of drag measurements. Model A.

V mph.	h ins.	Drag lbs.	Wire Drag.	Press. Corrn.	Model Drag.	k_f	$R/10^6$
No screen.							
20	0.34	.0152	.0017	.0020	.0115	.00298	0.538
30	0.69	.0308	.0038	.0045	.0225	.00258	0.807
40	1.15	.0514	.0066	.0077	.0371	.00240	1.076
50	1.67	.0746	.0102	.0117	.0527	.00218	1.345
60	2.33	.1041	.0148	.0160	.0733	.00211	1.614
Screen 1. Position (1).							
20	0.32	.0143	.0017	.0024	.0102	.00264	0.538
30	0.68	.0304	.0038	.0052	.0214	.00246	0.807
40	1.14	.0510	.0066	.0090	.0354	.00229	1.076
50	1.76	.0787	.0102	.0133	.0552	.00232	1.345
60	2.53	.1131	.0148	.0178	.0805	.00231	1.614
Position (2).							
20	0.31	.0139	.0017	.0003	.0119	.00308	0.538
30	0.71	.0317	.0038	.0007	.0272	.00312	0.807
40	1.36	.0608	.0066	.0013	.0529	.00342	1.076
50	2.17	.0970	.0102	.0016	.0852	.00353	1.345
60	3.23	.1444	.0148	.0016	.1280	.00368	1.614
Position (3).							
20	0.39	.0174	.0017	-.0011	.0168	.00435	0.538
30	0.96	.0429	.0038	-.0026	.0417	.00478	0.807
40	1.72	.0768	.0066	-.0046	.0748	.00484	1.076
50	2.63	.1185	.0102	-.0075	.1158	.00479	1.345
60	3.73	.1668	.0148	-.0114	.1634	.00469	1.614
Position (4).							
20	0.63	.0282	.0017	.0012	.0253	.00654	0.538
30	1.38	.0617	.0038	.0013	.0566	.00650	0.807
40	2.35	.1050	.0066	-.0007	.0991	.00640	1.076
50	3.50	.1654	.0102	-.0060	.1522	.00630	1.345
60	4.75	.2121	.0148	-.0163	.2136	.00614	1.614

Table 3. Results of drag measurements. Model A.

Screen 2. Position (1).

W mph.	h ins.	Drag lbs.	Wire Drag.	Press. Corrn.	Model Drag	k_f	$R/10^6$
20	0.31	.0139	.0017	.0006	.0116	.00300	0.538
30	0.62	.0277	.0038	.0012	.0227	.00261	0.807
40	1.01	.0451	.0066	.0019	.0366	.00237	1.076
50	1.48	.0662	.0102	.0026	.0534	.00221	1.345
60	2.07	.0925	.0148	.0032	.0745	.00214	1.614
		Position (2).					
20	0.23	.0103	.0017	-.0024	.0110	.00285	0.538
30	0.47	.0210	.0038	-.0055	.0227	.00261	0.807
40	0.82	.0367	.0066	-.0098	.0399	.00258	1.076
50	1.39	.0622	.0102	-.0153	.0673	.00279	1.345
60	2.13	.0952	.0148	-.0220	.1024	.00294	1.614
		Position (3).					
20	0.22	.0098	.0017	-.0032	.0113	.00292	0.538
30	0.60	.0268	.0038	-.0073	.0303	.00348	0.807
40	1.13	.0505	.0066	-.0138	.0572	.00370	1.076
50	1.83	.0818	.0102	-.0214	.0930	.00385	1.345
60	2.65	.1185	.0148	-.0319	.1356	.00390	1.614
		Position (4).					
20	0.64	.0286	.0017	.0032	.0237	.00613	0.538
30	1.38	.0617	.0038	.0058	.0521	.00598	0.807
40	2.23	.0997	.0066	.0076	.0855	.00553	1.076
50	3.28	.1465	.0102	.0071	.1292	.00535	1.345
60	4.42	.1975	.0148	.0028	.1799	.00517	1.614

Table 4. Results of drag measurements. Model A.

Screen 3. Position (1).

V mph.	h ins.	Drag lbs.	Wire Drag.	Press. Corrn.	Model Drag.	k_f	$R/10^6$
20	0.33	.0147	.0017	.0012	.0118	.00305	0.538
30	0.66	.0295	.0038	.0026	.0231	.00265	0.807
40	1.08	.0483	.0066	.0043	.0374	.00242	1.076
50	1.59	.0711	.0102	.0062	.0547	.00286	1.345
60	2.18	.0975	.0148	.0080	.0747	.00215	1.614
		Position (2).					
20	0.23	.0103	.0017	-.0001	.0087	.00225	0.538
30	0.53	.0237	.0038	-.0002	.0201	.00231	0.807
40	0.91	.0407	.0066	-.0006	.0347	.00224	1.076
50	1.35	.0604	.0102	-.0012	.0514	.00213	1.345
60	1.89	.0845	.0148	-.0023	.0720	.00207	1.614
		Position (3).					
20	0.31	.0139	.0017	-.0003	.0125	.00324	0.538
30	0.65	.0291	.0038	-.0009	.0262	.00301	0.807
40	1.17	.0523	.0066	-.0018	.0475	.00307	1.076
50	1.93	.0863	.0102	-.0035	.0796	.00330	1.345
60	2.82	.1260	.0148	-.0063	.1175	.00337	1.614
		Position (4).					
20	0.57	.0255	.0017	.0016	.0222	.00574	0.538
30	1.28	.0572	.0038	.0032	.0502	.00576	0.807
40	2.18	.0975	.0066	.0049	.0860	.00556	1.076
50	3.16	.1411	.0102	.0054	.1255	.00519	1.345
60	4.35	.1943	.0148	.0039	.1756	.00504	1.614

Table 5. Results of drag measurements. Model B.

No screen.

V mph.	h ins.	Drag lbs.	Wire Drag.	Press. Corrn.	Model Drag.	k_f	$R/10^6$
20	0.43	.0205	.0017	.0023	.0165	.00377	0.538
30	0.72	.0343	.0038	.0049	.0256	.00260	0.807
40	1.31	.0625	.0066	.0084	.0475	.00271	1.076
50	2.26	.1079	.0102	.0120	.0857	.00313	1.345
60	3.35	.1599	.0148	.0153	.1298	.00329	1.614
Screen 1. Position (1).							
20	0.34	.0162	.0017	.0026	.0119	.00272	0.538
30	0.81	.0386	.0038	.0057	.0291	.00295	0.807
40	1.53	.0730	.0066	.0096	.0568	.00324	1.076
50	2.46	.1173	.0102	.0137	.0934	.00342	1.345
60	3.32	.1584	.0148	.0180	.1256	.00319(?)	1.614
Position (2).							
20	0.35	.0167	.0017	.0002	.0148	.00338	0.538
30	0.87	.0415	.0038	.0005	.0372	.00377	0.807
40	1.57	.0749	.0066	.0007	.0676	.00386	1.076
50	2.49	.1188	.0102	.0005	.1081	.00395	1.345
60	3.56	.1698	.0148	-.0002	.1552	.00394	1.614
Position (3).							
20	0.44	.0210	.0017	-.0015	.0208	.00475	0.538
30	1.02	.0486	.0038	-.0033	.0481	.00488	0.807
40	1.81	.0864	.0066	-.0060	.0858	.00490	1.076
50	2.76	.1316	.0102	-.0099	.1313	.00480	1.345
60	3.85	.1836	.0148	-.0151	.1839	.00467	1.614
Position (4).							
20	0.64	.0305	.0017	.0014	.0274	.00626	0.538
30	1.45	.0692	.0038	.0017	.0637	.00646	0.807
40	2.45	.1169	.0066	-.0004	.1107	.00632	1.076
50	3.70	.1765	.0102	-.0074	.1737	.00635	1.345
60	4.98	.2377	.0148	-.0208	.2437	.00618	1.614

Table 6. Results of drag measurements. Model B.

Screen 2. Position (1).

V mph.	h ins.	Drag lbs.	Wire Drag.	Press. Corrn.	Model Drag.	k_f	$R/10^6$
20	0.33	.0157	.0017	.0004	.0136	.00311	0.538
30	0.67	.0320	.0038	.0009	.0273	.00277	0.807
40	1.34	.0639	.0066	.0014	.0559	.00319	1.076
50	2.16	.1030	.0102	.0014	.0914	.00334	1.345
60	3.09	.1474	.0148	.0006	.1320	.00335	1.614
		Position (2).					
20	0.27	.0129	.0017	-.0030	.0142	.00325	0.538
30	0.70	.0334	.0038	-.0069	.0365	.00370	0.807
40	1.25	.0596	.0066	-.0121	.0651	.00372	1.076
50	1.93	.0921	.0102	-.0190	.1009	.00369	1.345
60	2.72	.1297	.0148	-.0273	.1422	.00361	1.614
		Position (3).					
20	0.30	.0143	.0017	-.0040	.0166	.00379	0.538
30	0.75	.0358	.0038	-.0091	.0411	.00417	0.807
40	1.31	.0625	.0066	-.0166	.0725	.00414	1.076
50	1.99	.0950	.0102	-.0266	.1114	.00407	1.345
60	2.81	.1340	.0148	-.0395	.1587	.00403	1.614
		Position (4).					
20	0.70	.0334	.0017	.0034	.0283	.00647	0.538
30	1.48	.0706	.0038	.0060	.0608	.00617	0.807
40	2.39	.1140	.0066	.0072	.1002	.00572	1.076
50	3.44	.1640	.0102	.0056	.1482	.00542	1.345
60	4.58	.2184	.0148	-.0007	.2043	.00519	1.614

Table 7. Results of drag measurements. Model B.

Screen 3. Position (1).

V mph.	h ins.	Drag lbs.	Wire Drag.	Press. Corrn.	Model Drag.	k_f	$R/10^6$
20	0.36	.0172	.0017	.0013	.0142	.00324	0.538
30	0.68	.0324	.0038	.0027	.0259	.00263	0.807
40	1.24	.0592	.0066	.0043	.0483	.00276	1.076
50	2.14	.1020	.0102	.0055	.0863	.00315	1.345
60	3.12	.1488	.0148	.0059	.1281	.00325	1.614
		Position (2).					
20	0.30	.0143	.0017	-.0003	.0129	.00295	0.538
30	0.65	.0310	.0038	-.0007	.0279	.00283	0.807
40	1.30	.0620	.0066	-.0015	.0569	.00325	1.076
50	2.11	.1006	.0102	-.0030	.0934	.00342	1.345
60	3.00	.1430	.0148	-.0055	.1337	.00339	1.614
		Position (3).					
20	0.32	.0153	.0017	-.0006	.0142	.00324	0.538
30	0.86	.0410	.0038	-.0015	.0387	.00393	0.807
40	1.53	.0730	.0066	-.0036	.0694	.00396	1.076
50	2.32	.1106	.0102	-.0056	.1066	.00387	1.345
60	3.27	.1560	.0148	-.0095	.1507	.00383	1.614
		Position (4).					
20	0.59	.0281	.0017	.0020	.0244	.00557	0.538
30	1.34	.0639	.0038	.0037	.0564	.00572	0.807
40	2.22	.1059	.0066	.0049	.0944	.00539	1.076
50	3.27	.1560	.0102	.0049	.1409	.00515	1.345
60	4.48	.2137	.0148	.0026	.1963	.00498	1.614

MODEL 'A'
MODEL 'B'
L = 35"
Max. Diameter
D = 7"
Max. Diameter
D = 7"
13.66"
14.00"
Y
X

FIG. 1.

Arrangement of model tests

Screen No.	a	b	c	d	
1	8 69	5.39	3.35	1.42	ft
2	8.69	4 86	3.41	1.48	"
3	8 69	5.39	3.35	1.51	

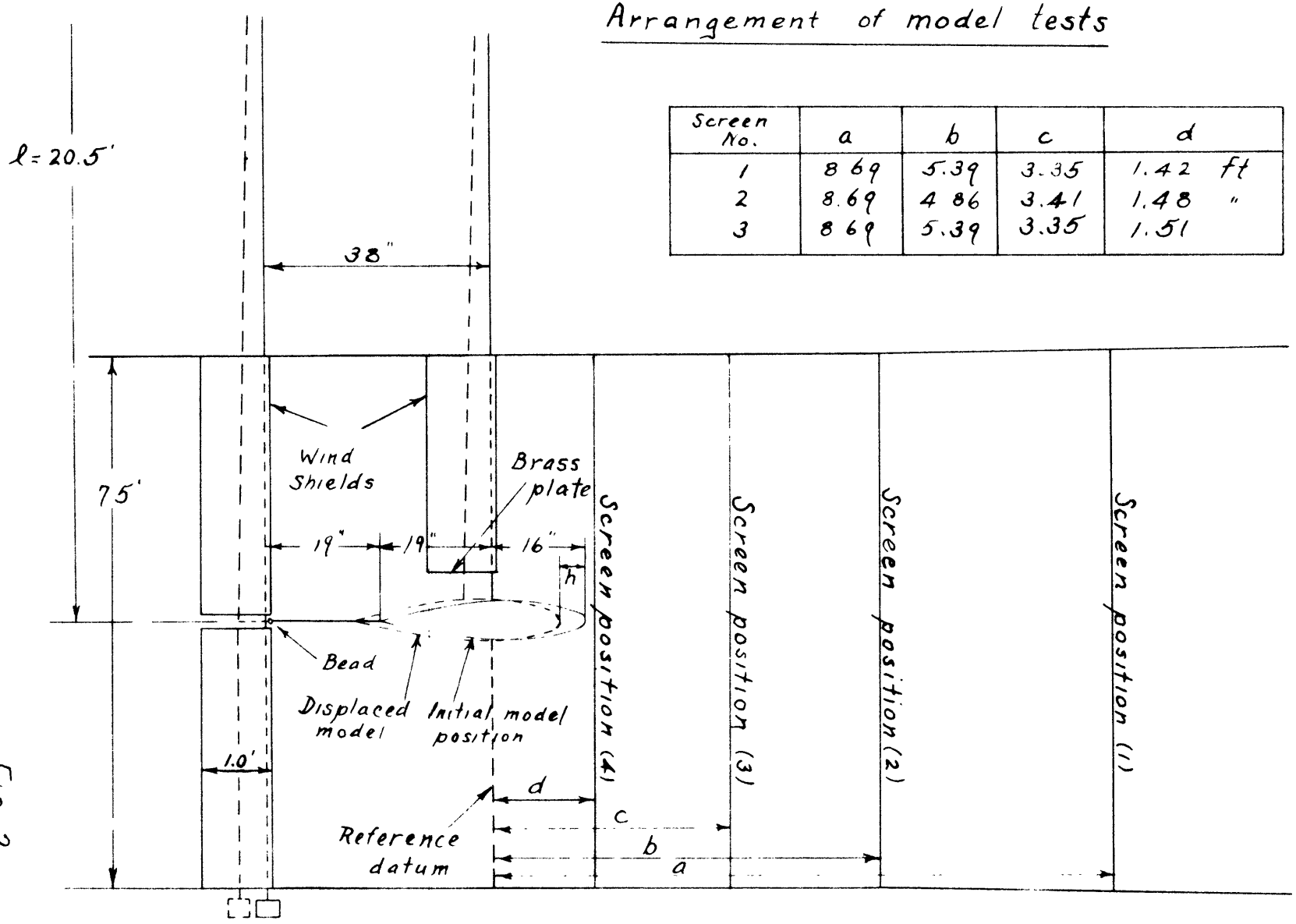

FIG. 2.

Arrangement of sphere tests.

Screen No.	a	b	c	d	e
1	8.69	5.39	3.35	1.42	0.58 ft.
2	8.69	4.86	3.41	1.48	0.60 "
3	8.69	5.39	3.35	1.51	0.55 "

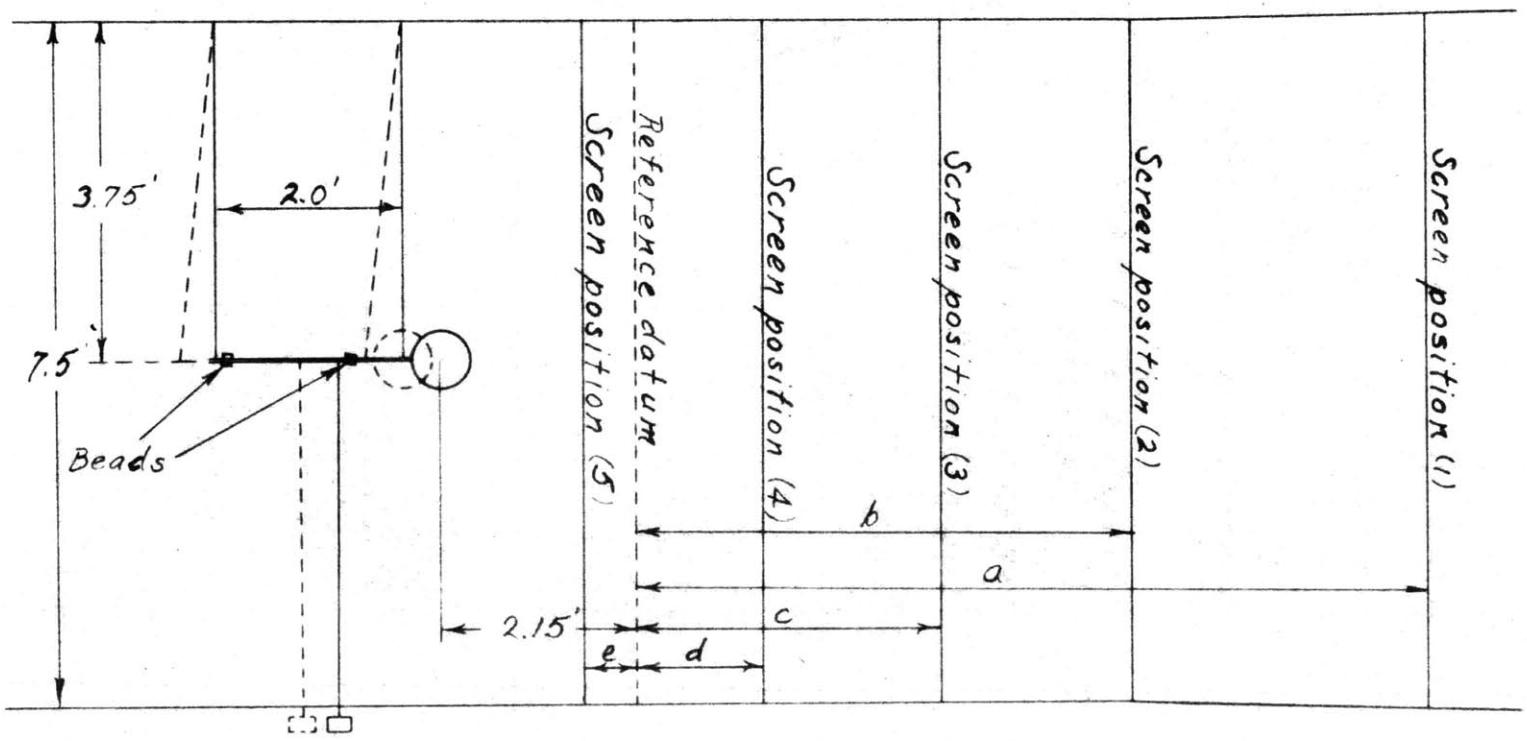

FIG. 3.

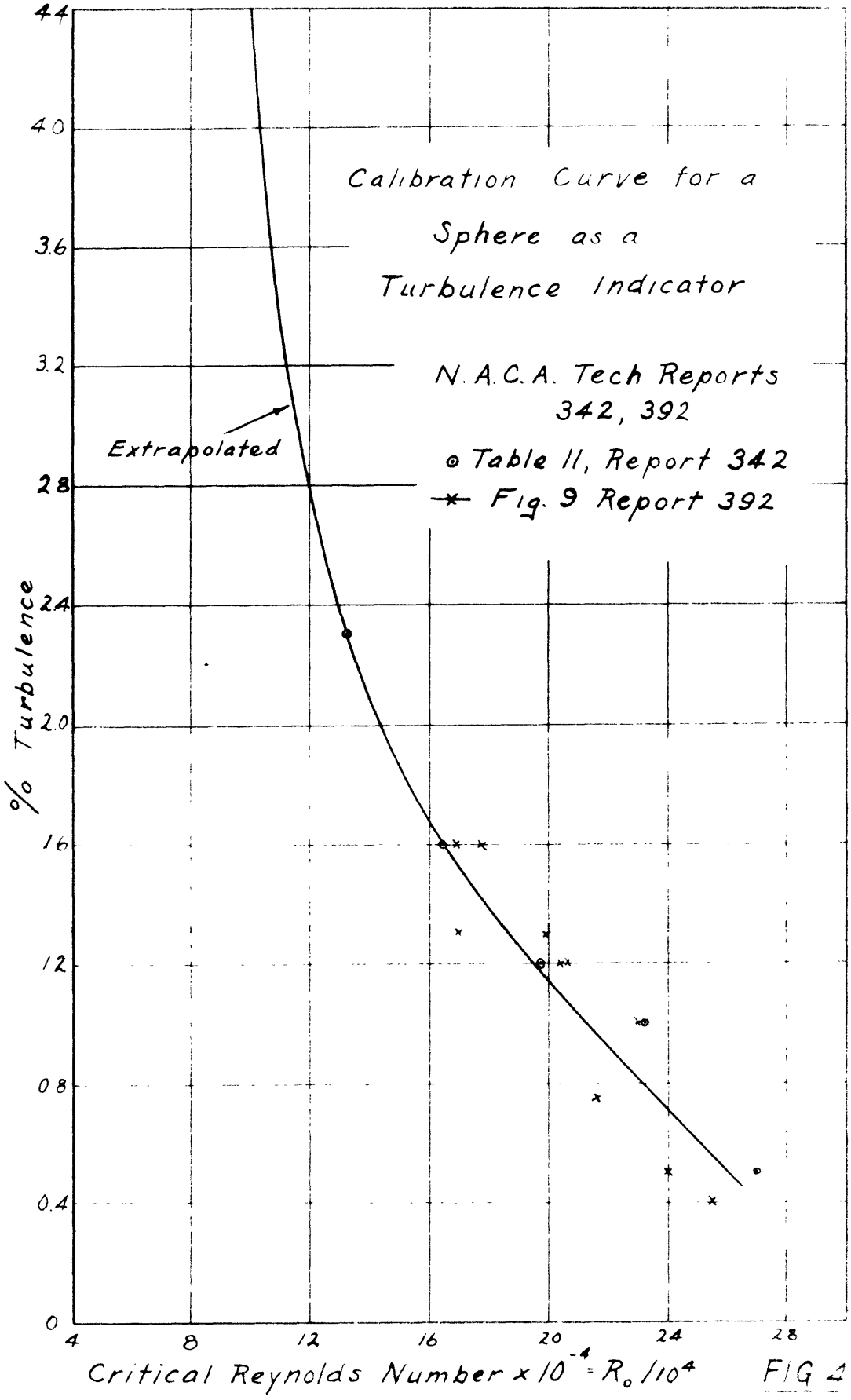
Calibration Curve for a
Sphere as a
Turbulence Indicator
N.A.C.A. Tech Reports
342, 392
⊙ Table II, Report 342
× Fig. 9 Report 392
Extrapolated
% Turbulence
0
0.4
0.8
1.2
1.6
2.0
2.4
2.8
3.2
3.6
4.0
4.4
4
8
12
16
20
24
28
Critical Reynolds Number x 10⁻⁴ = R₀/10⁴

FIG 2

Drag Coefficient of 78" Sphere behind Screen 1.

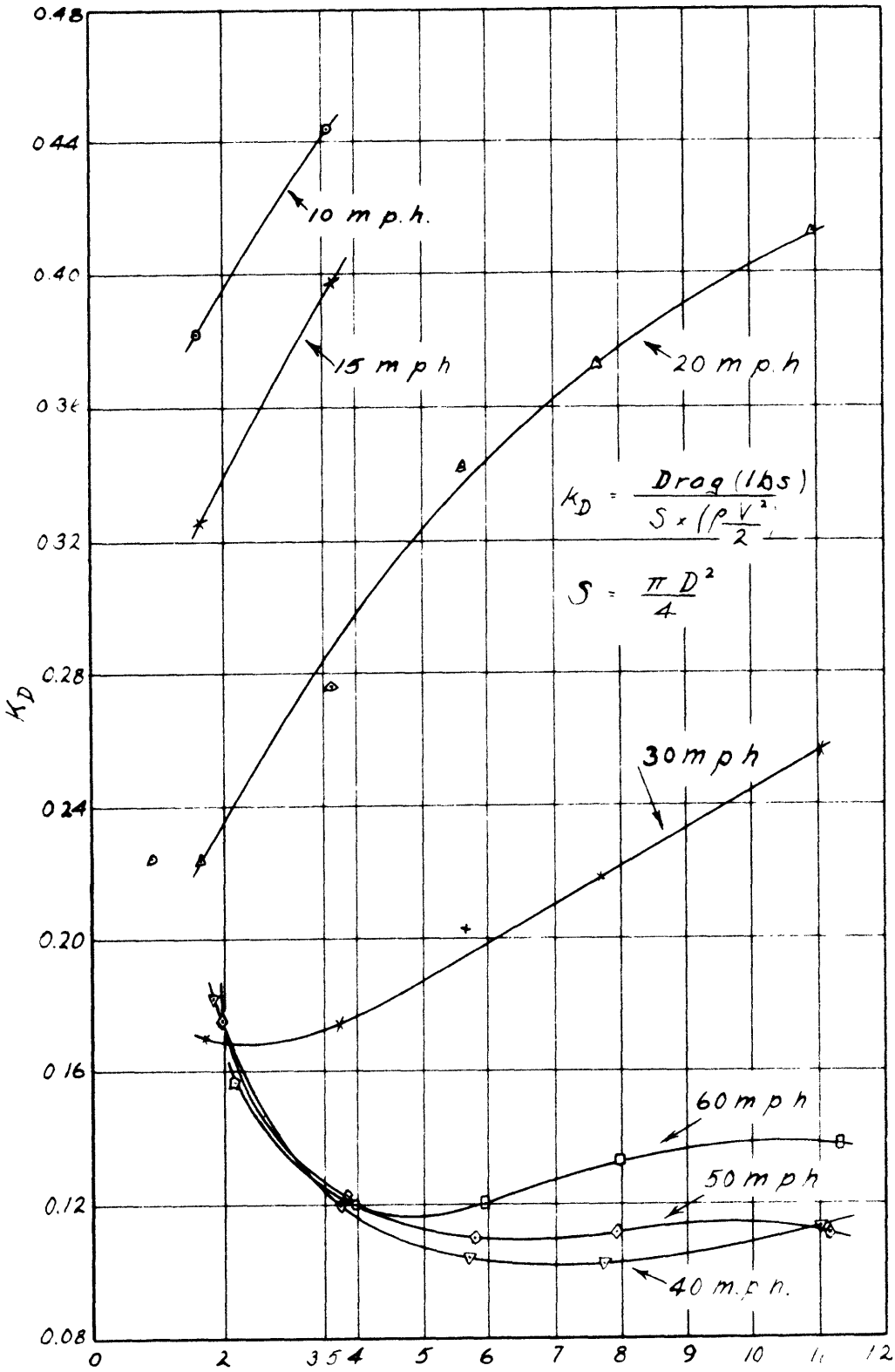

FIG 5.

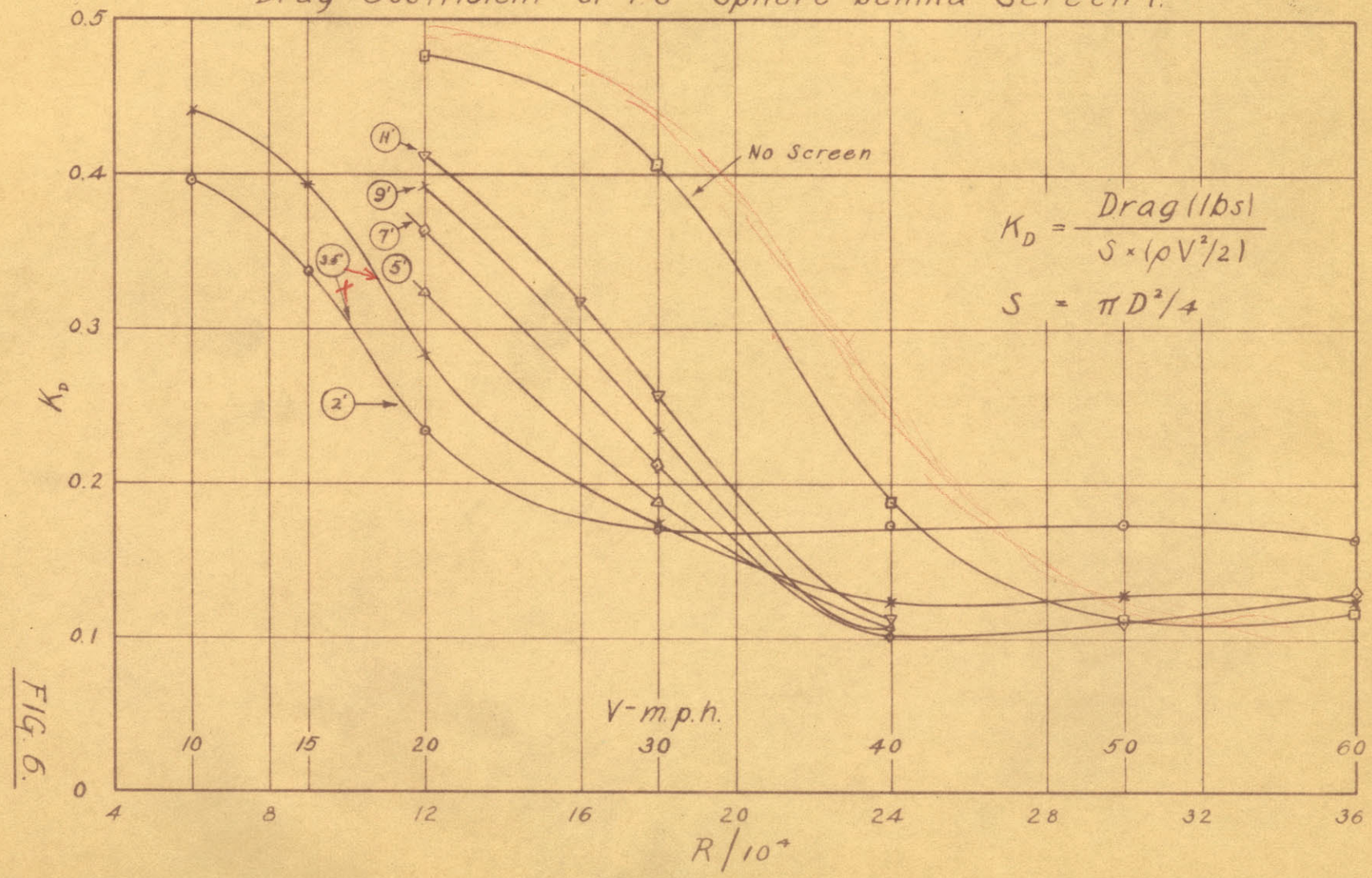
Drag Coefficient of 7.8" Sphere behind Screen 1.
No Screen
11'
9'
7'
5'
3.5'
2'
$K_D = \frac{Drag\ (lbs)}{S \times (\rho V^2/2)}$
$S = \pi D^2/4$
K_D
V-m.p.h.
10
15
20
30
40
50
60
0
0.1
0.2
0.3
0.4
0.5
4
8
12
16
20
24
28
32
36
$R/10^4$

FIG. 6.

Drag Coefficients of 7.8" Sphere behind Screen 2

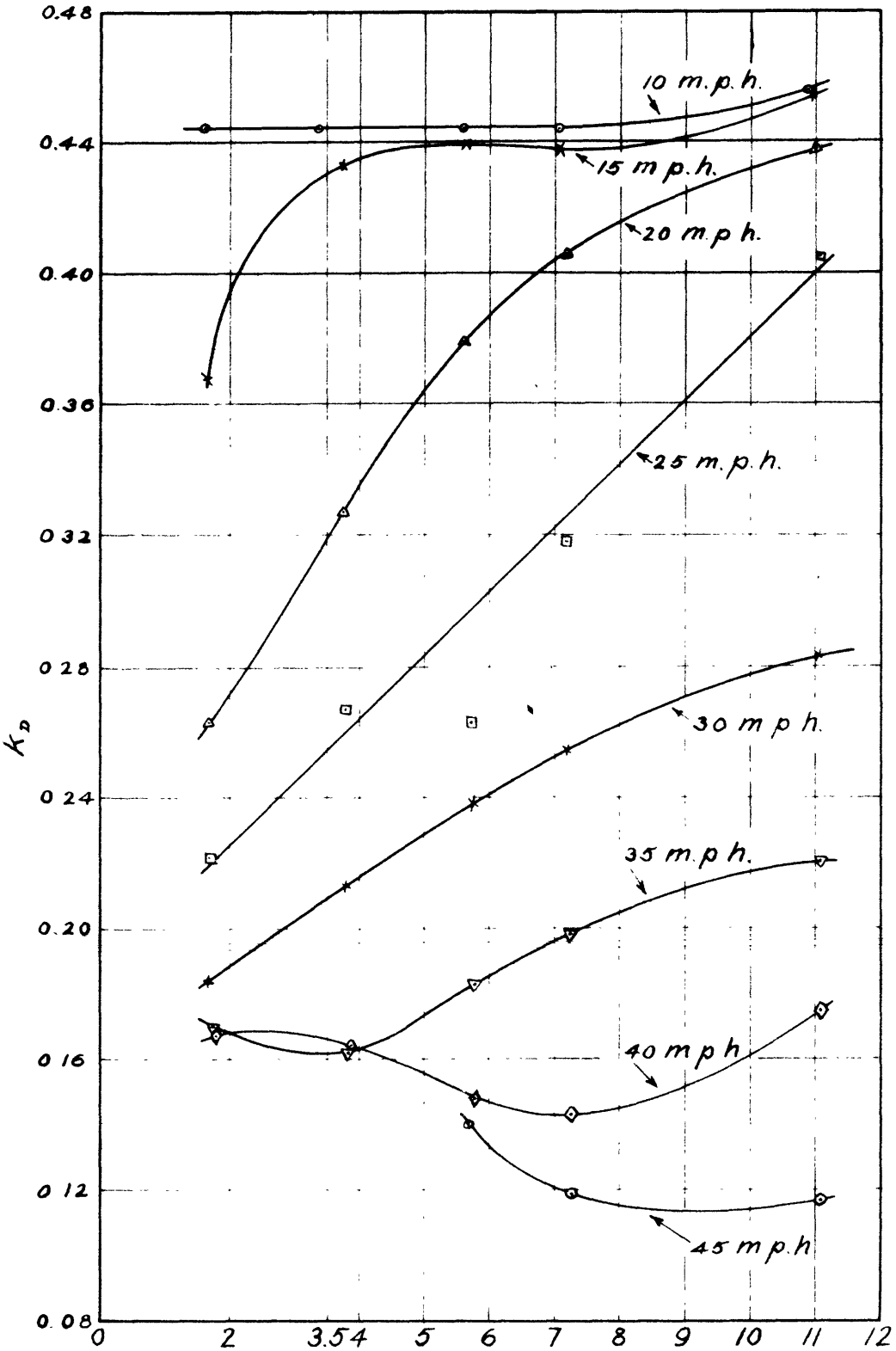

FIG. 7

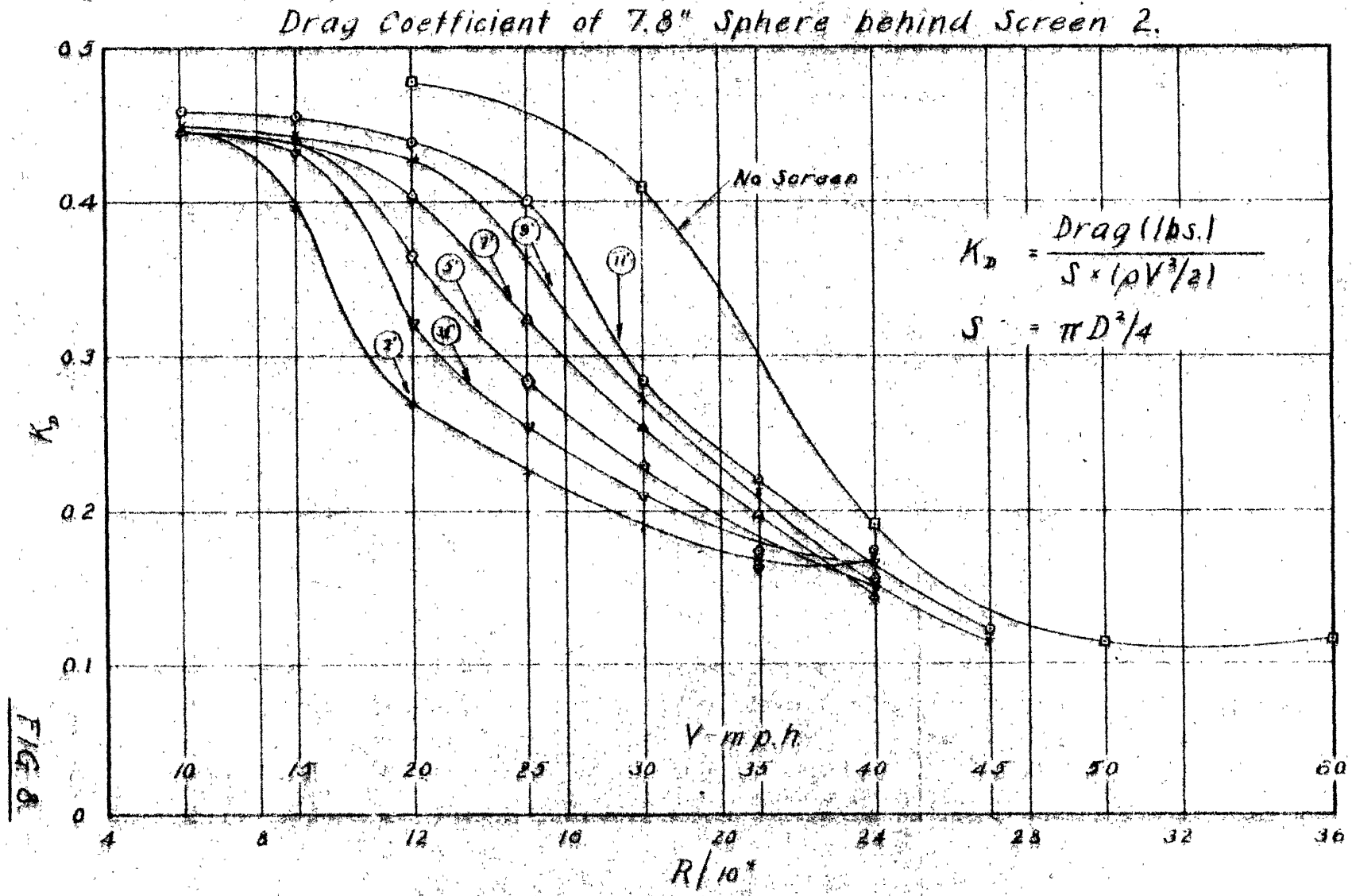
Drag Coefficient of 7.8" Sphere behind Screen 2.
No Screen
$K_D = \frac{Drag\ (lbs.)}{S \times (\rho V^2/2)}$
$S = \pi D^2/4$
K_D
V - m.p.h
R / 10^4
FIG 6

Drag Coefficients of 7.8" Sphere behind Screen 3.

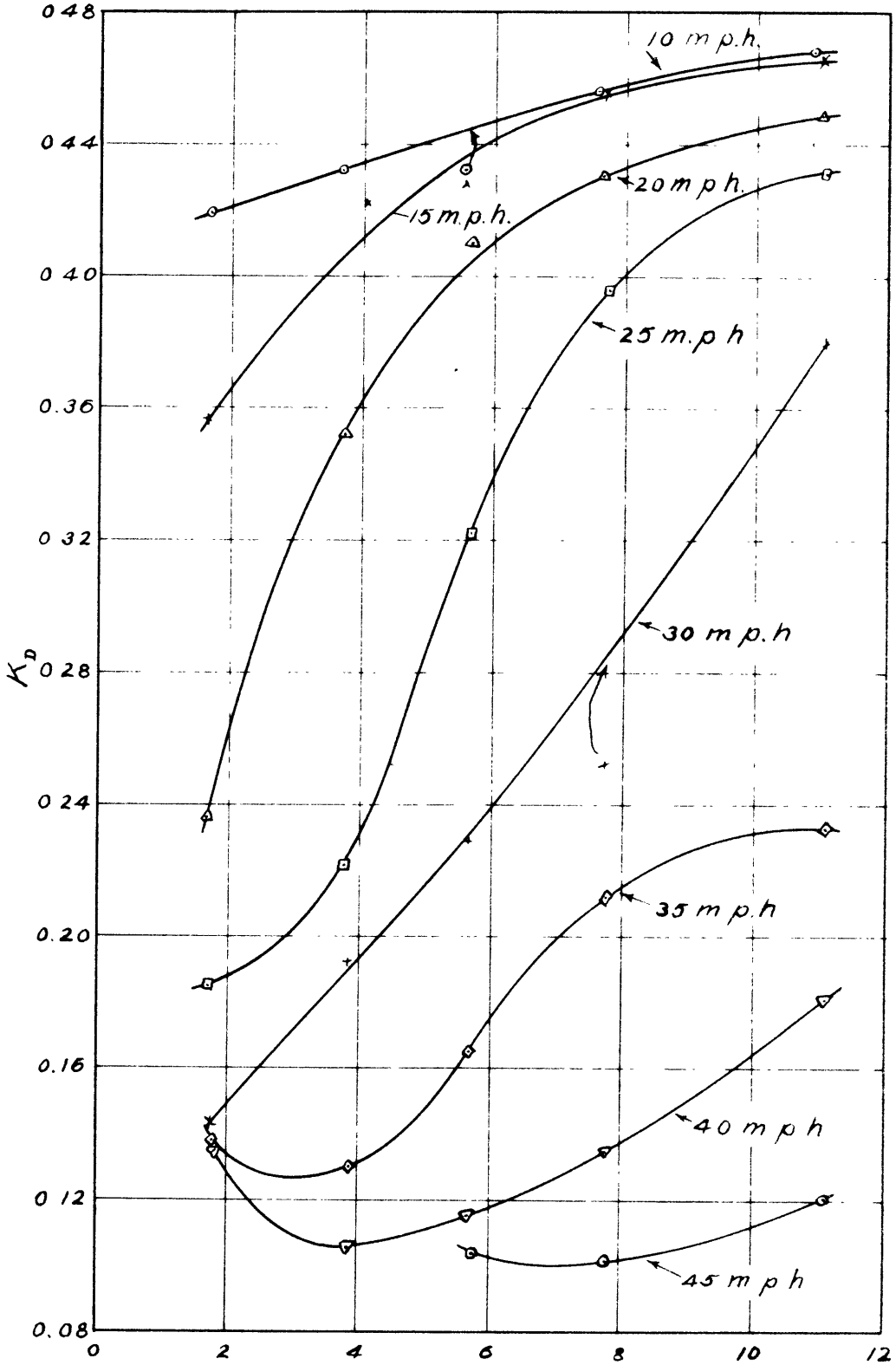

FIG 9

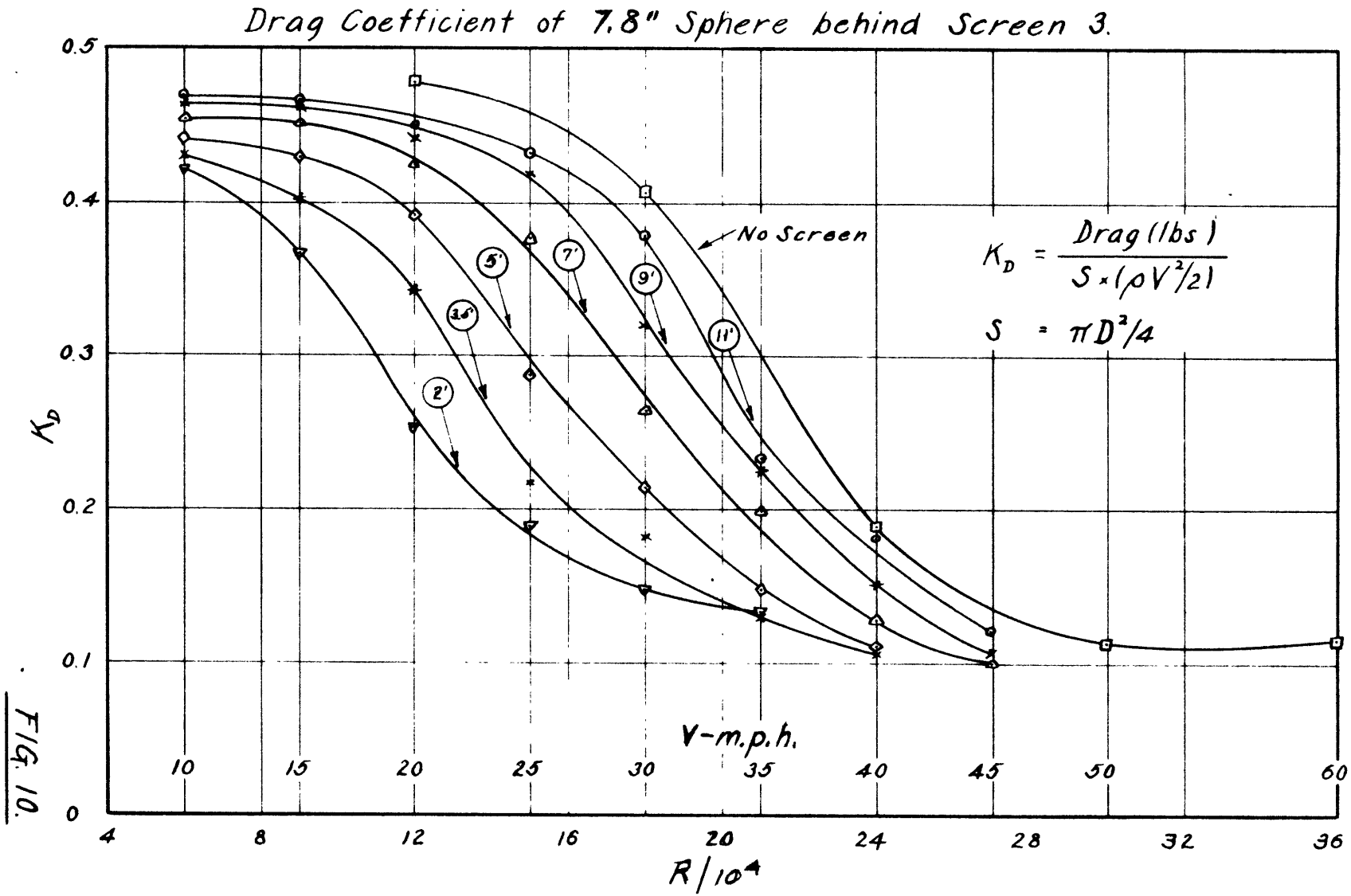
Drag Coefficient of 7.8" Sphere behind Screen 3.
0.5
0.4
0.3
0.2
0.1
0
K_D
No Screen
2'
3.5'
5'
7'
9'
11'
$K_D = \frac{Drag\ (lbs)}{S \times (\rho V^2/2)}$
$S = \pi D^2/4$
V-m.p.h.
10
15
20
25
30
35
40
45
50
60
4
8
12
16
20
24
28
32
36
$R/10^4$

FIG. 10.

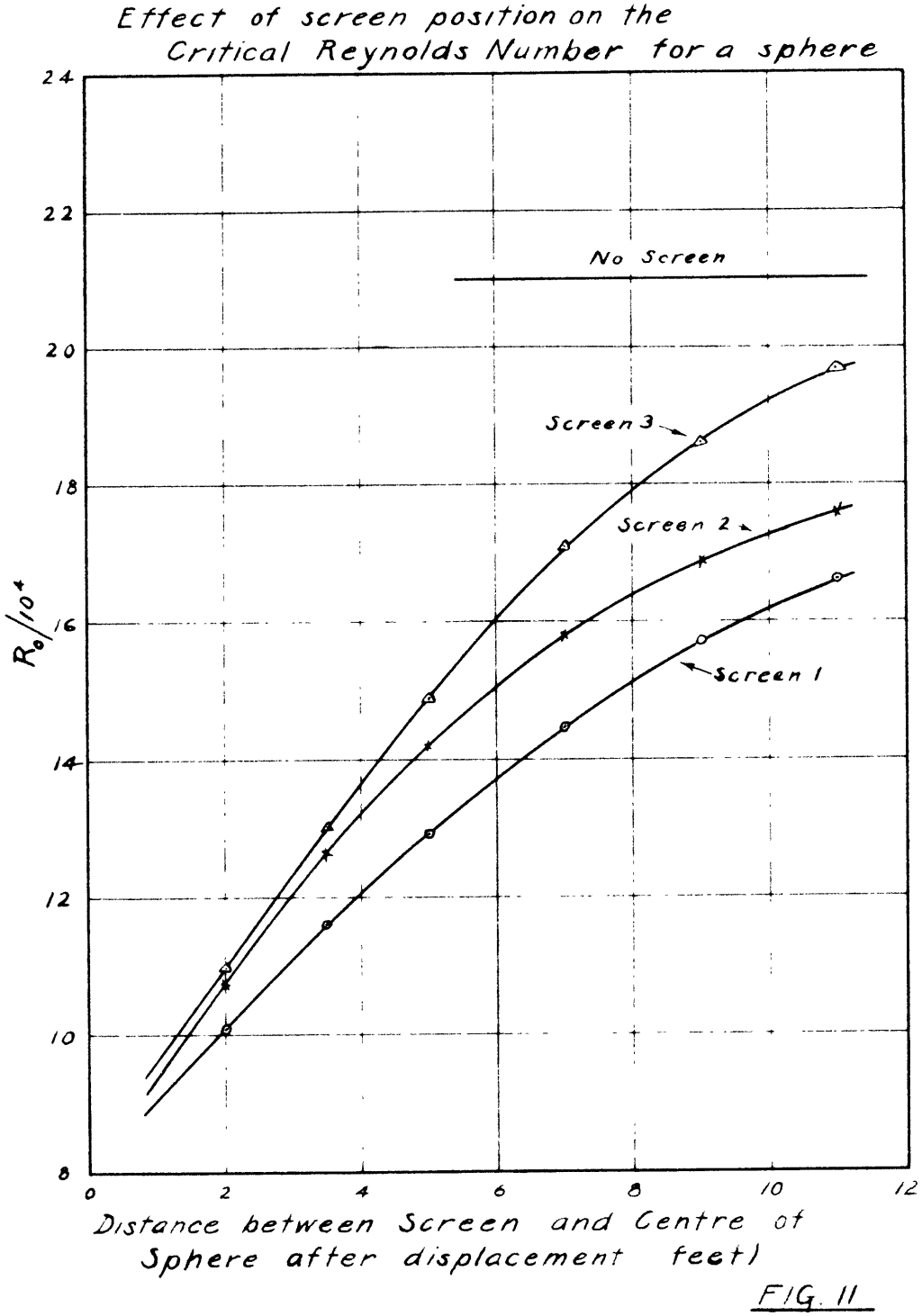
Effect of screen position on the
Critical Reynolds Number for a sphere
24
22
20
18
16
14
12
10
8
$R_0/10^4$
No Screen
Screen 3
Screen 2
Screen 1
0
2
4
6
8
10
12
Distance between Screen and Centre of
Sphere after displacement feet)

FIG. 11

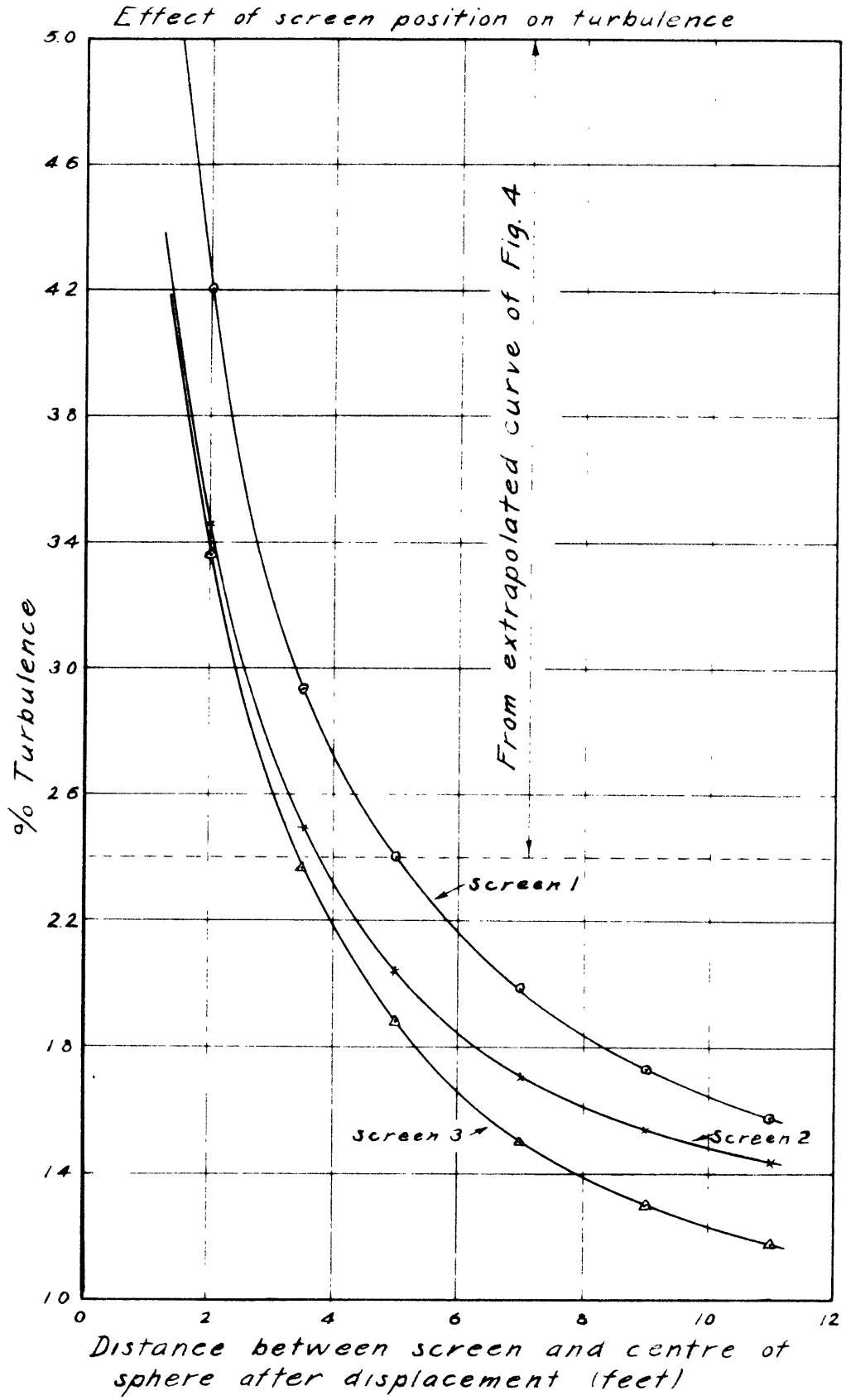
Effect of screen position on turbulence
5.0
4.6
4.2
3.8
3.4
3.0
2.6
2.2
1.8
1.4
1.0
% Turbulence
From extrapolated curve of Fig. 4
Screen 1
Screen 2
Screen 3
0
2
4
6
8
10
12
Distance between screen and centre of sphere after displacement (feet)

FIG. 12.

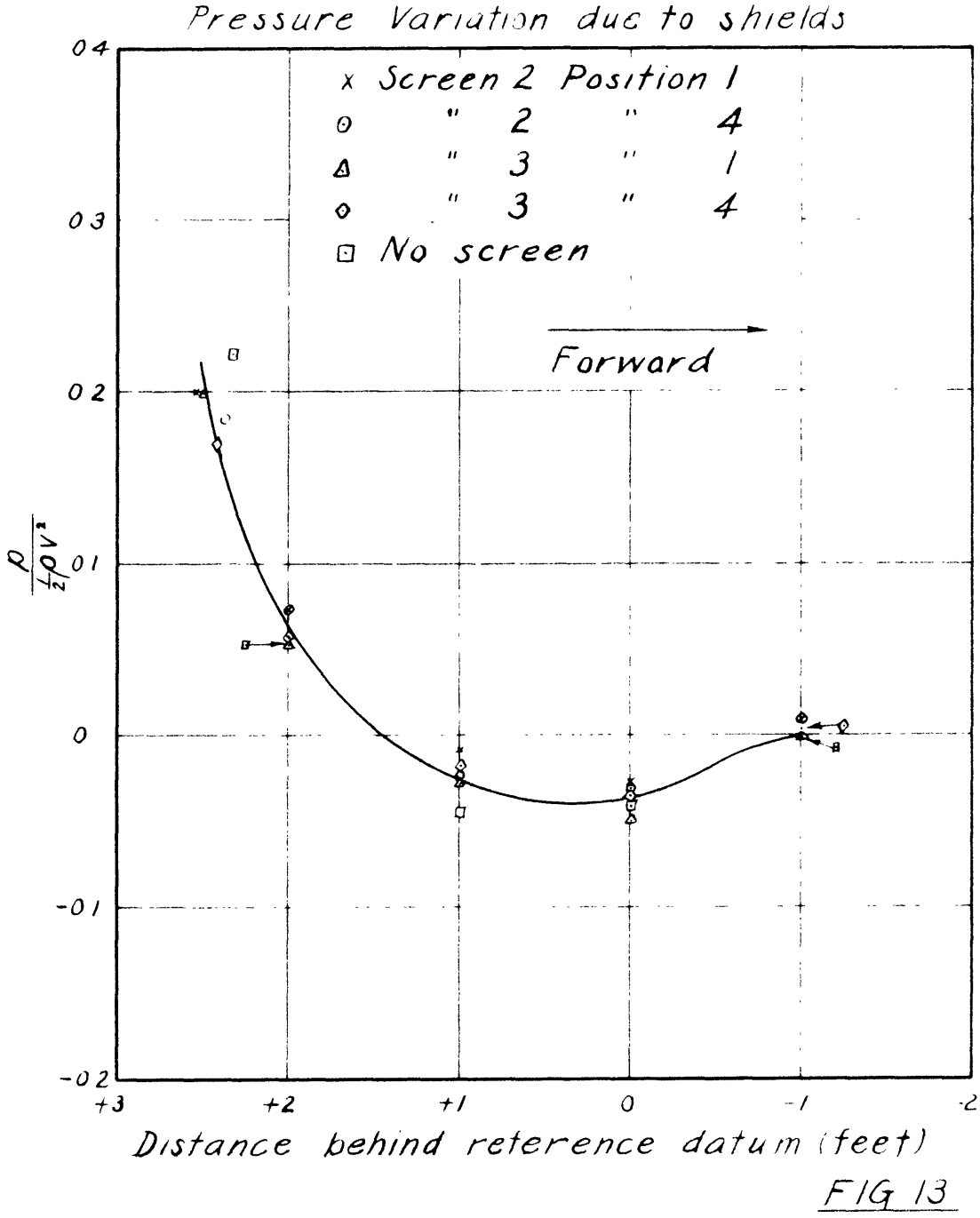
Pressure Variation due to shields
x Screen 2 Position 1
o " 2 " 4
Δ " 3 " 1
◇ " 3 " 4
□ No screen
Forward
0·4
0·3
0·2
0·1
0
-0·1
-0·2
+3
+2
+1
0
-1
-2
Distance behind reference datum (feet)

FIG 13

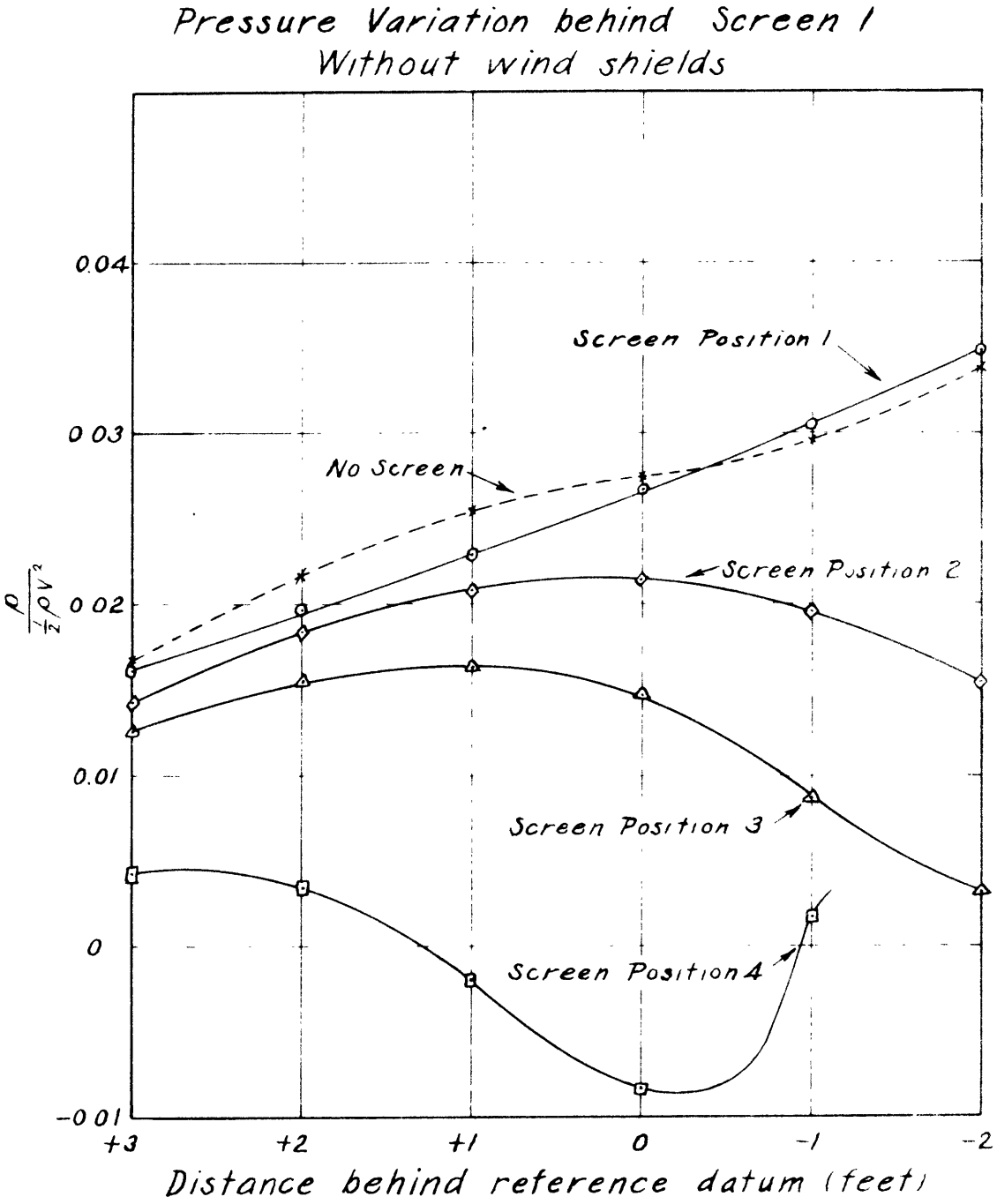
Pressure Variation behind Screen 1
Without wind shields
0.04
0 03
0 02
0.01
0
-0 01
$\frac{p}{\frac{1}{2}\rho V^2}$
Screen Position 1
No Screen
Screen Position 2
Screen Position 3
Screen Position 4
+3
+2
+1
0
-1
-2
Distance behind reference datum (feet)

FIG 14.

Pressure Variation behind Screen 1
With wind shields.

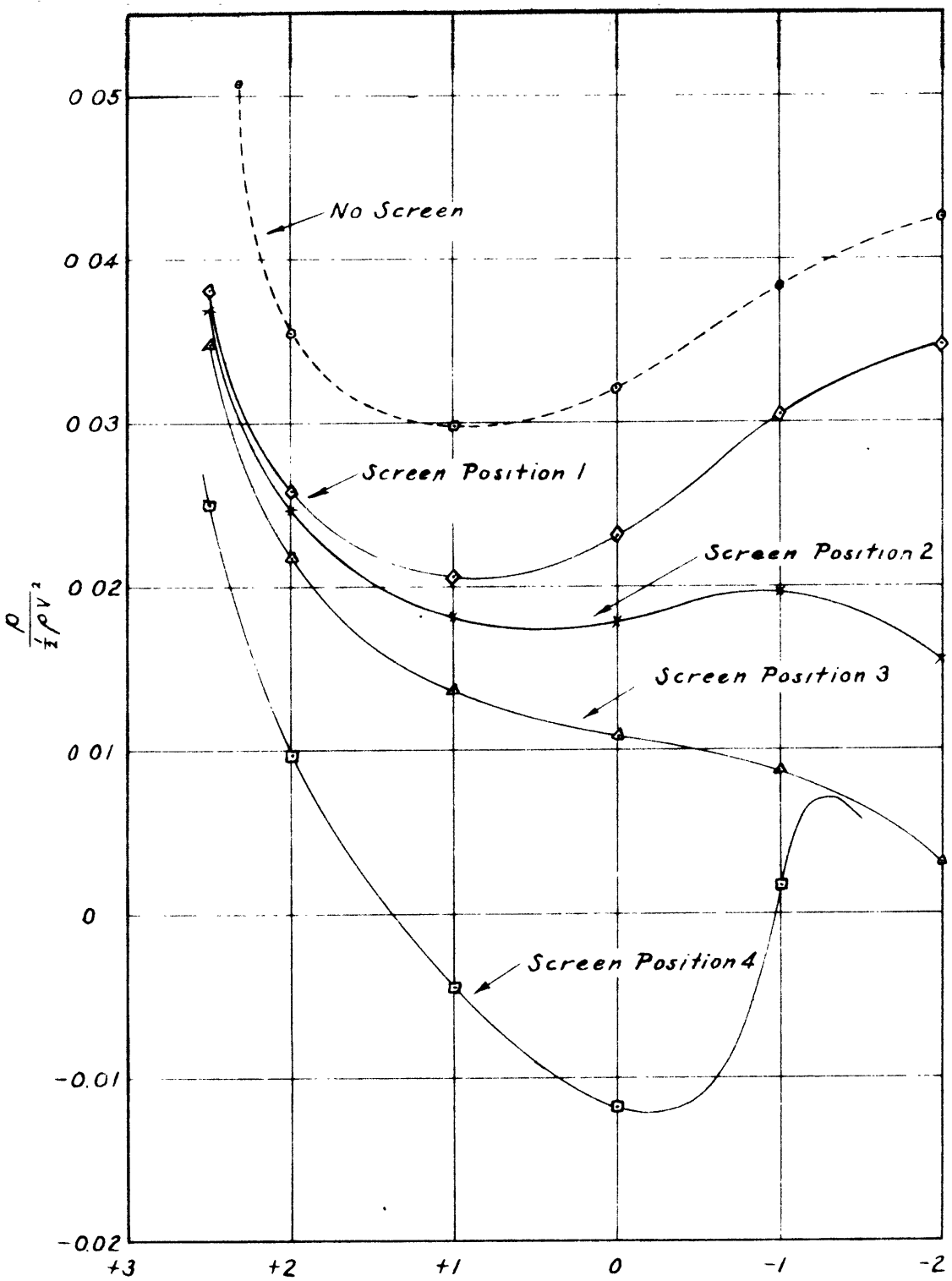

FIG. 15.

Pressure Variation behind Screen 2.
With wind shields

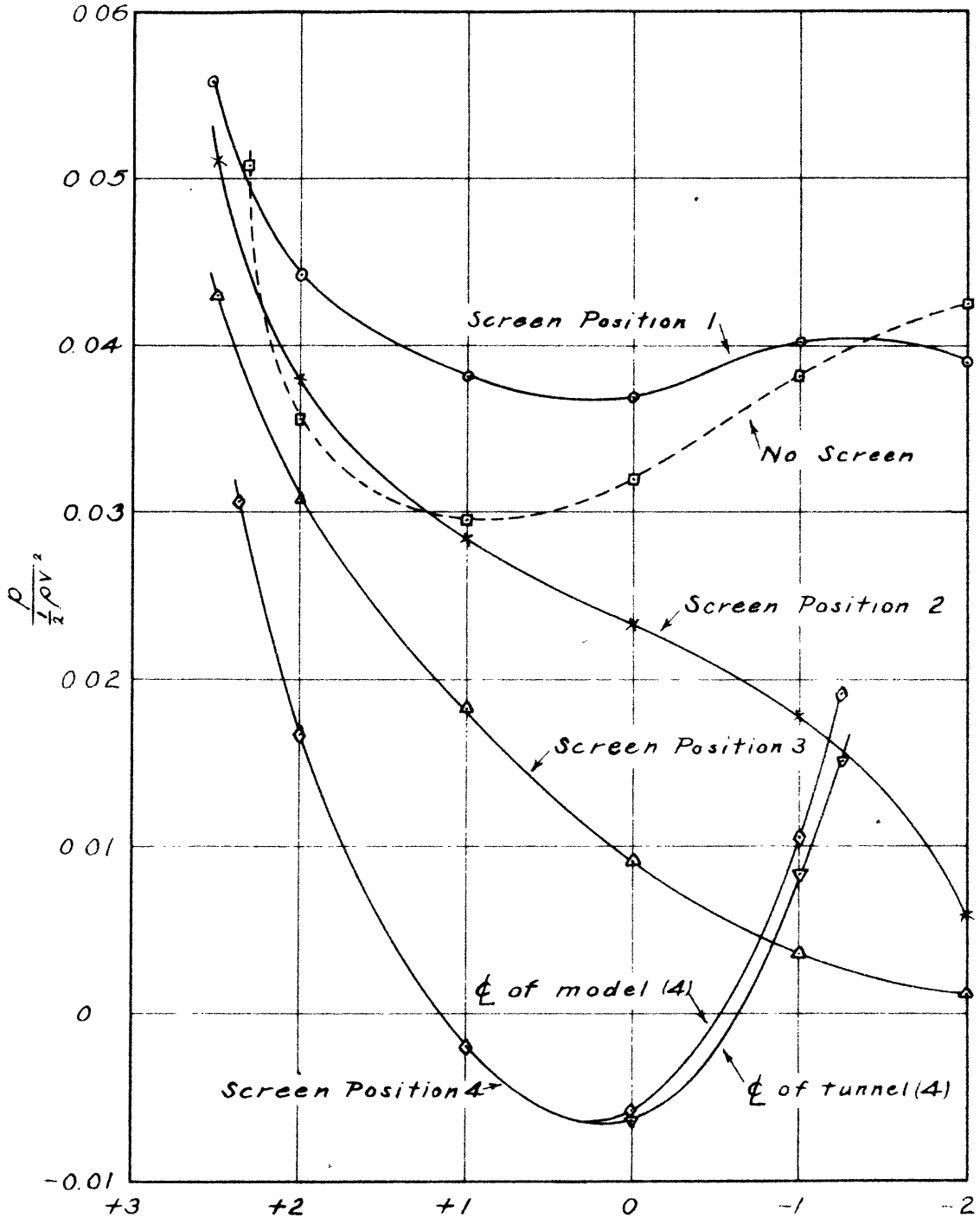

FIG. 16.

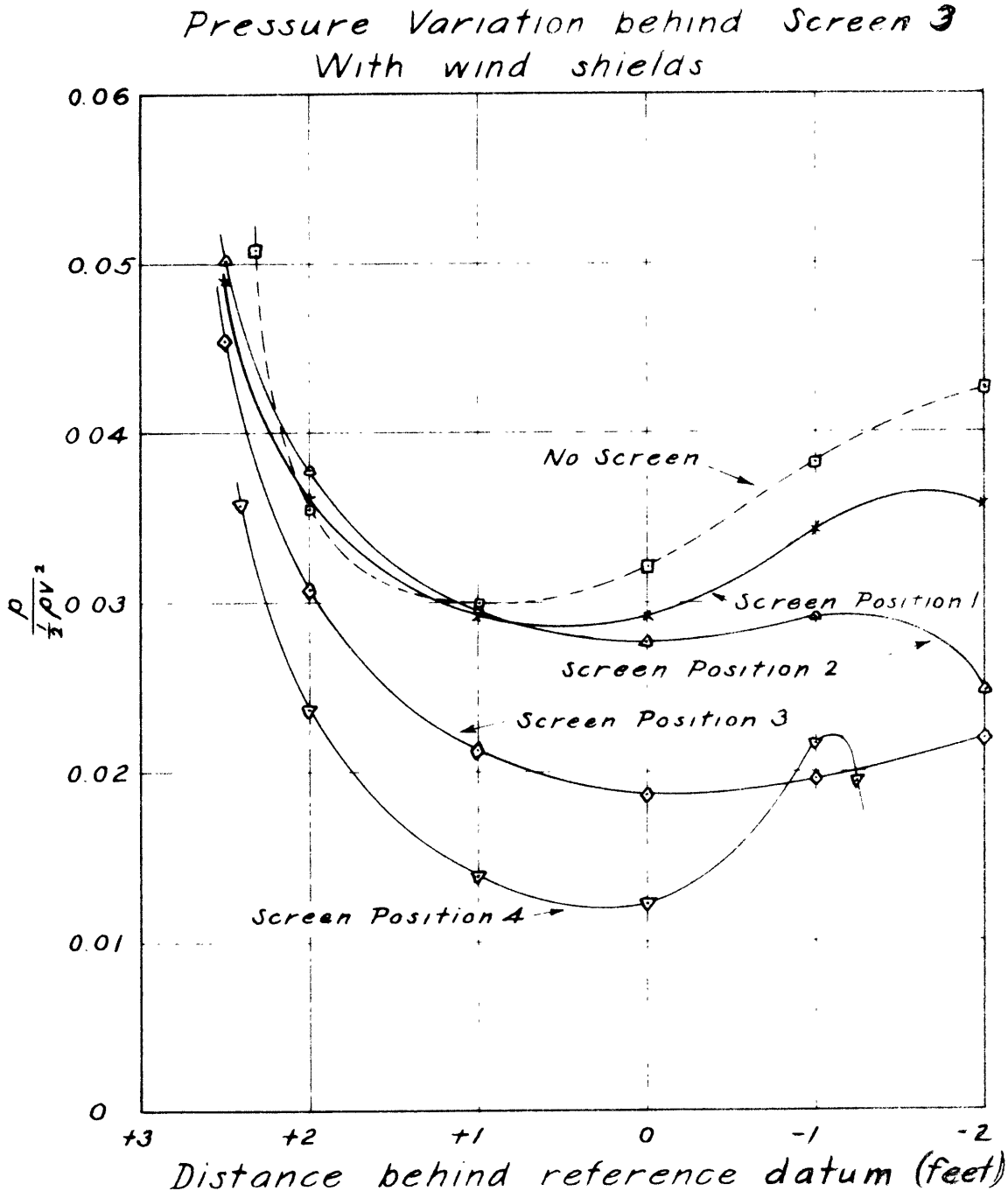
Pressure Variation behind Screen 3
With wind shields
0.06
0.05
0.04
0.03
0.02
0.01
0
$\frac{p}{\frac{1}{2}\rho V^2}$
No Screen
Screen Position 1
Screen Position 2
Screen Position 3
Screen Position 4
+3
+2
+1
0
-1
-2
Distance behind reference datum (feet)

FIG. 17.

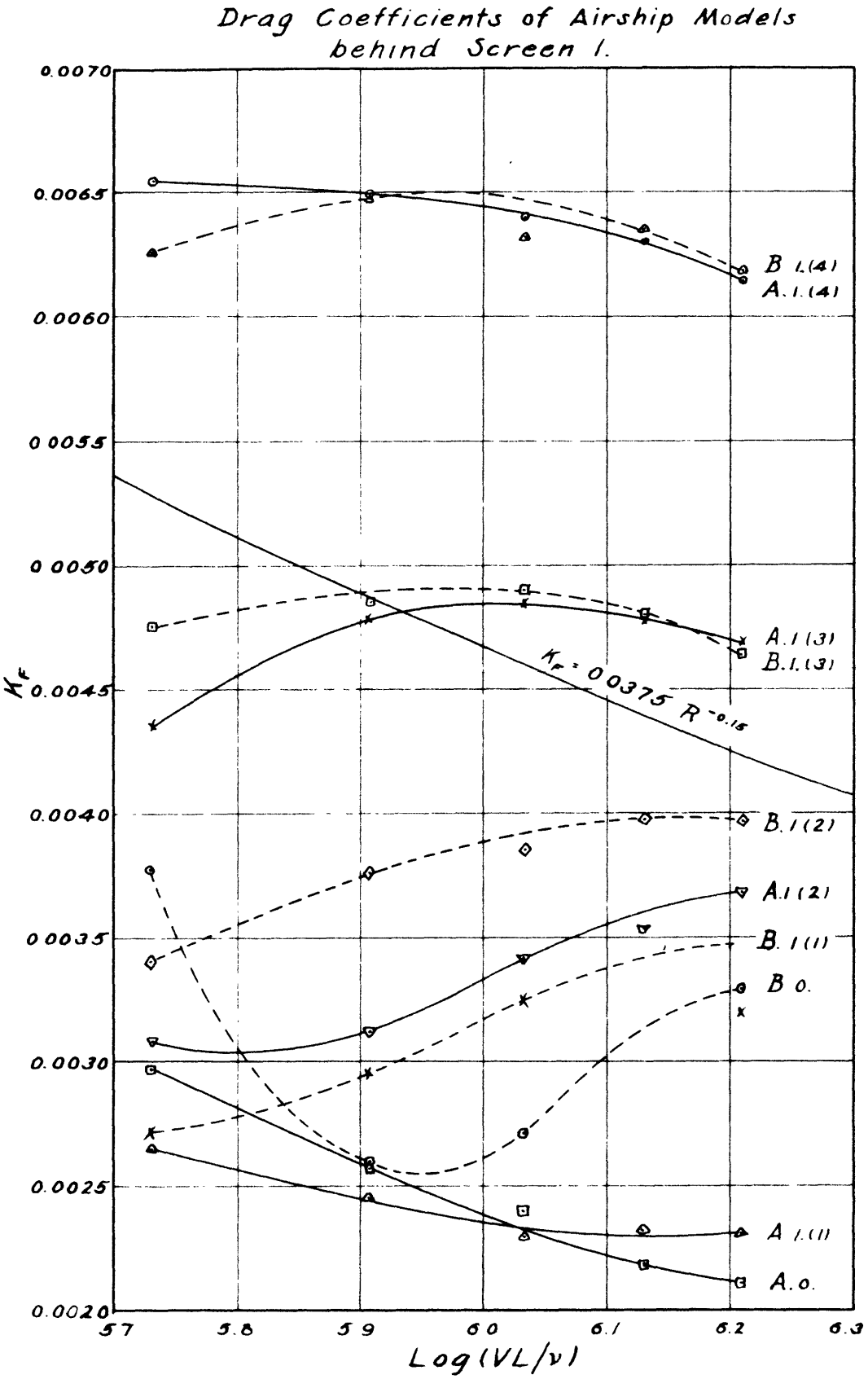

A 1 (3) = Model A, Screen 1, Position 3.

FIG. 18.

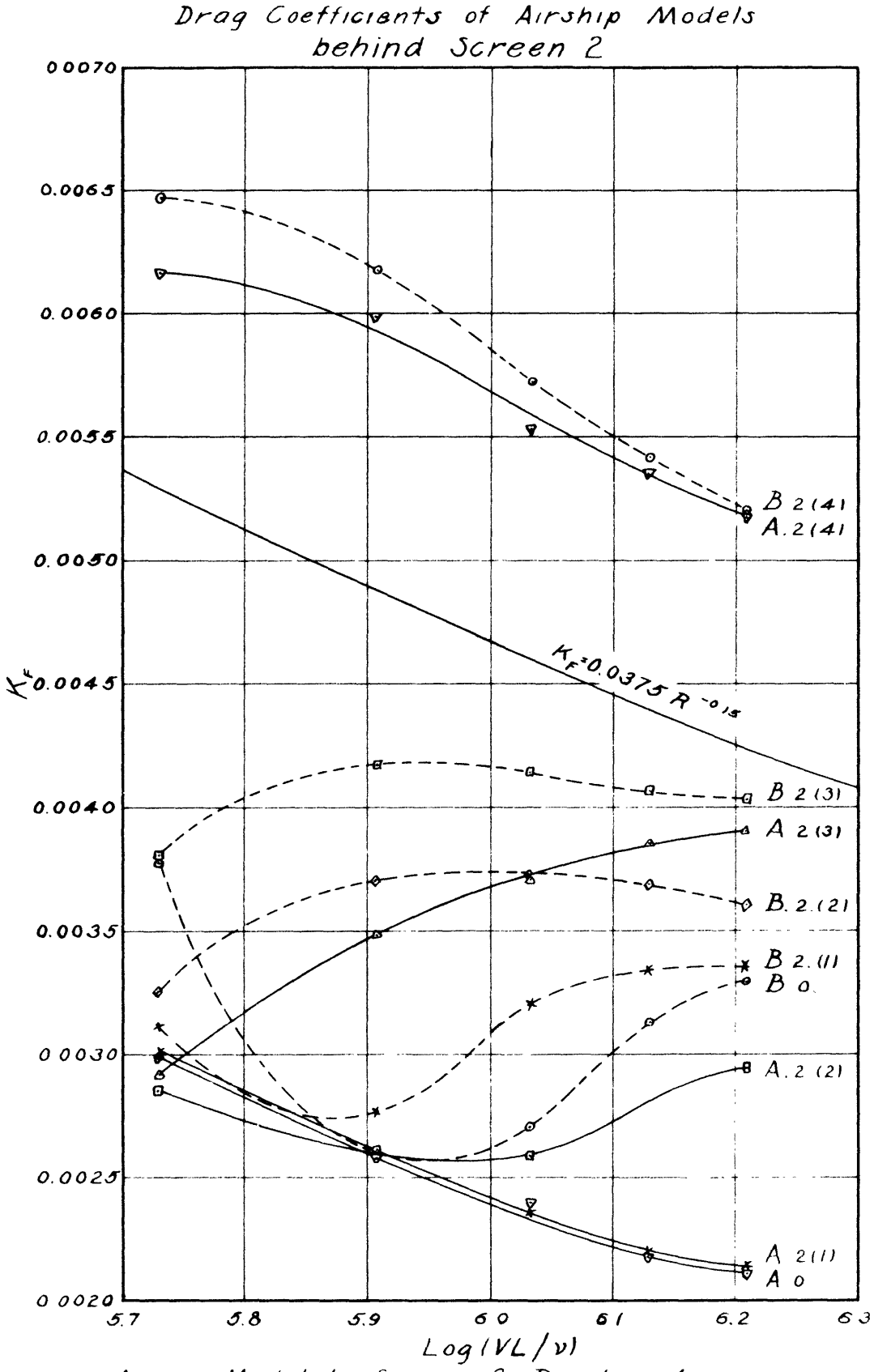

A 2 (4) = Model A, Screen 2, Position 4.

FIG. 19

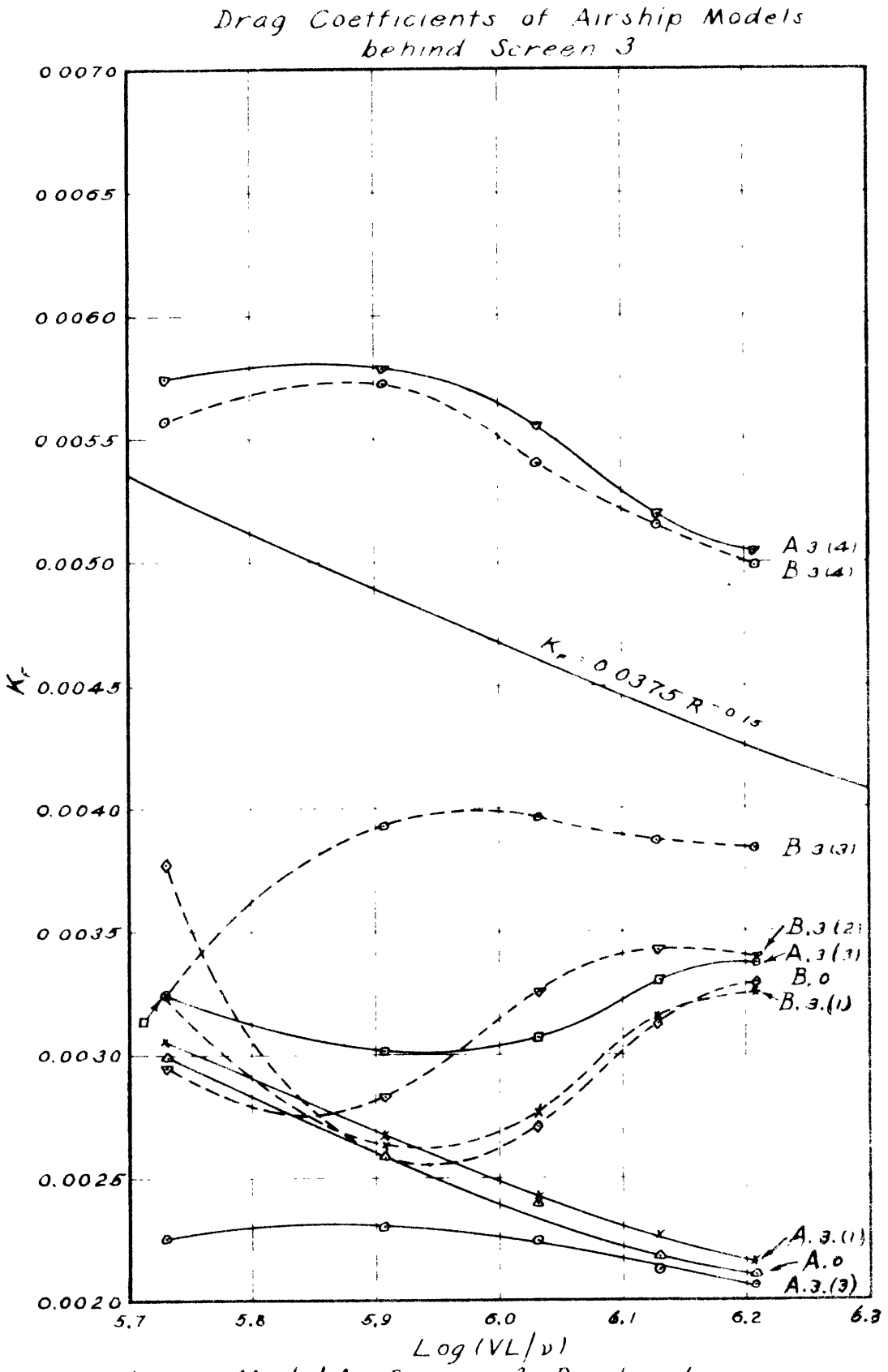

A. 3. (1) = Model A, Screen 3, Position 1.

FIG. 20.

Drag Coefficients of Airship Models and Flat Plates

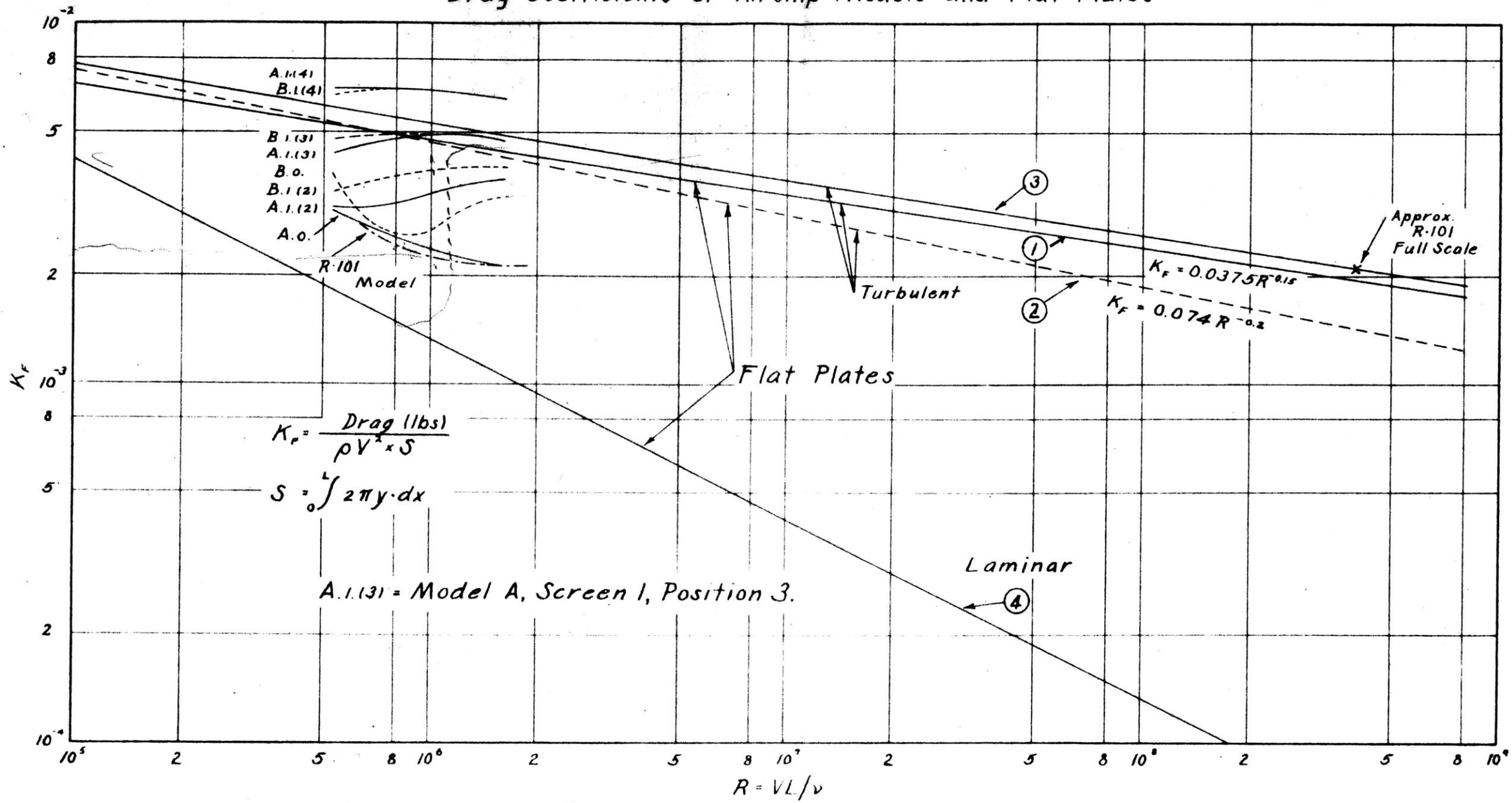

FIG. 21.

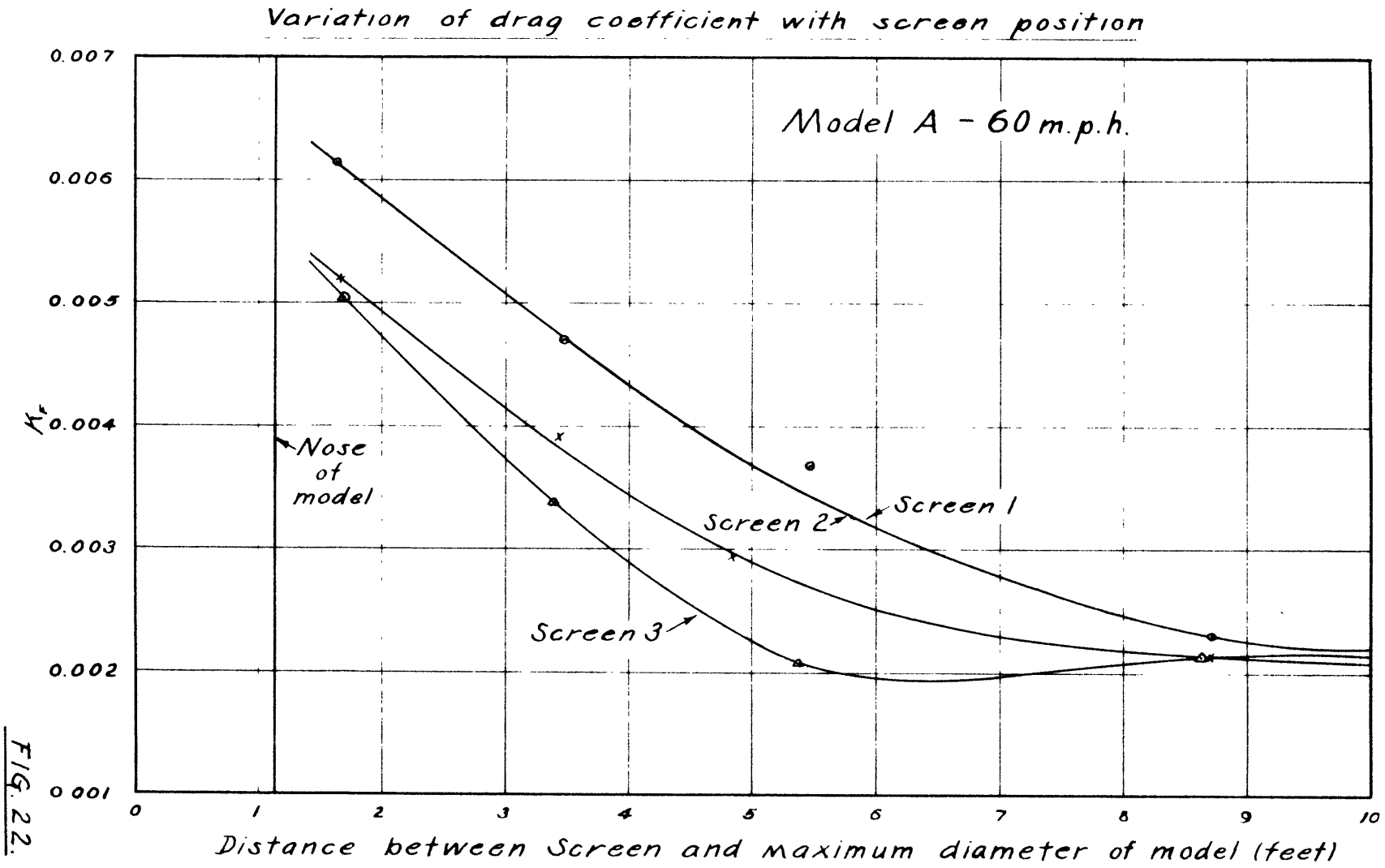
Variation of drag coefficient with screen position
Model A - 60 m.p.h.
0.007
0.006
0.005
0.004
0.003
0.002
0.001
K_x
Nose of model
Screen 1
Screen 2
Screen 3
0
1
2
3
4
5
6
7
8
9
10
Distance between Screen and maximum diameter of model (feet)

FIG. 22.

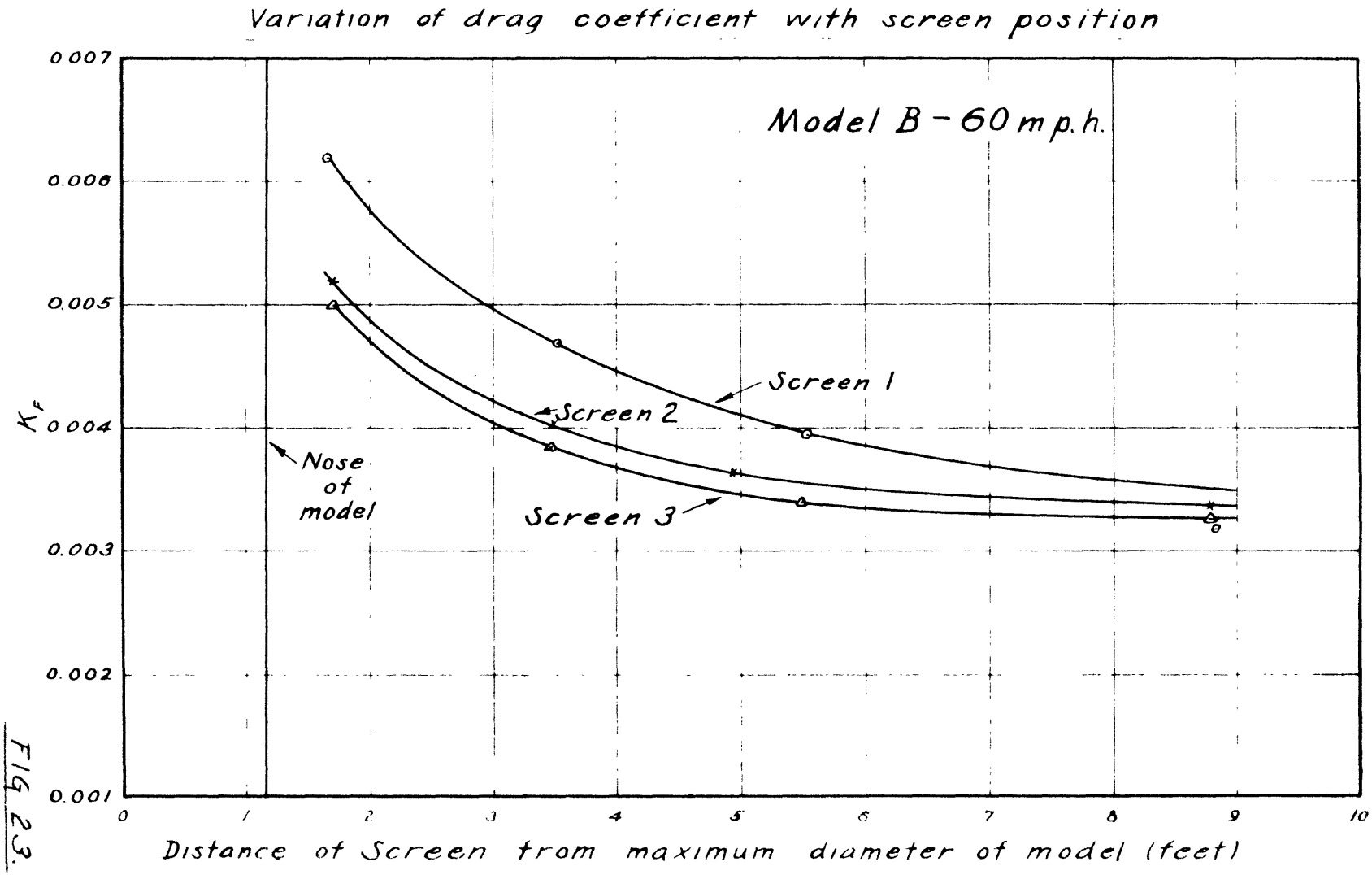
Variation of drag coefficient with screen position
Model B - 60 m.p.h.
Screen 1
Screen 2
Screen 3
Nose of model
K_F
0.007
0.006
0.005
0.004
0.003
0.002
0.001
0
1
2
3
4
5
6
7
8
9
10
Distance of Screen from maximum diameter of model (feet)

FIG 23.

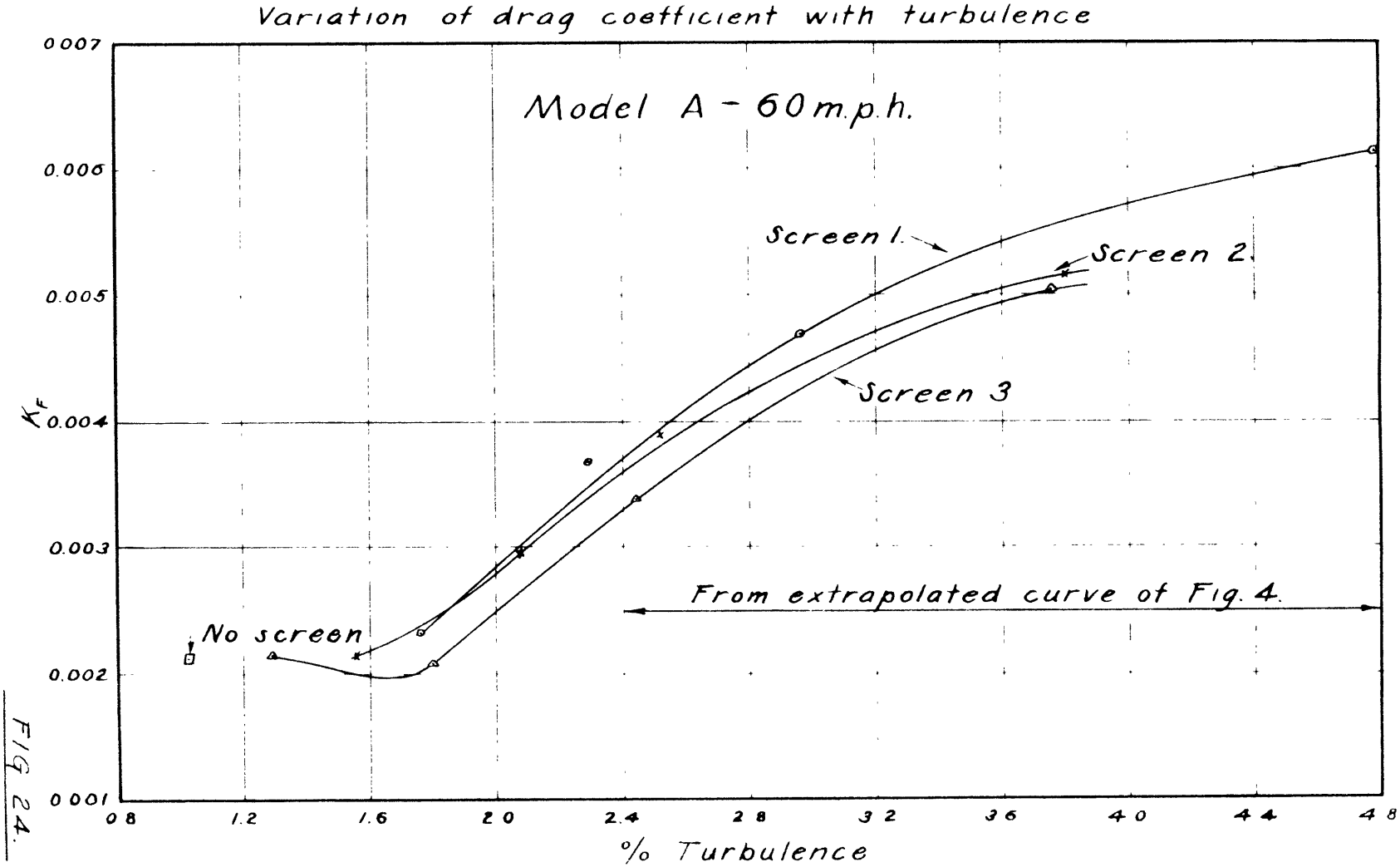
Variation of drag coefficient with turbulence
Model A - 60 m.p.h.
Screen 1.
Screen 2.
Screen 3
From extrapolated curve of Fig. 4.
No screen
K_F
0.007
0.006
0.005
0.004
0.003
0.002
0.001
0.8
1.2
1.6
2.0
2.4
2.8
3.2
3.6
4.0
4.4
4.8
% Turbulence

FIG 24.

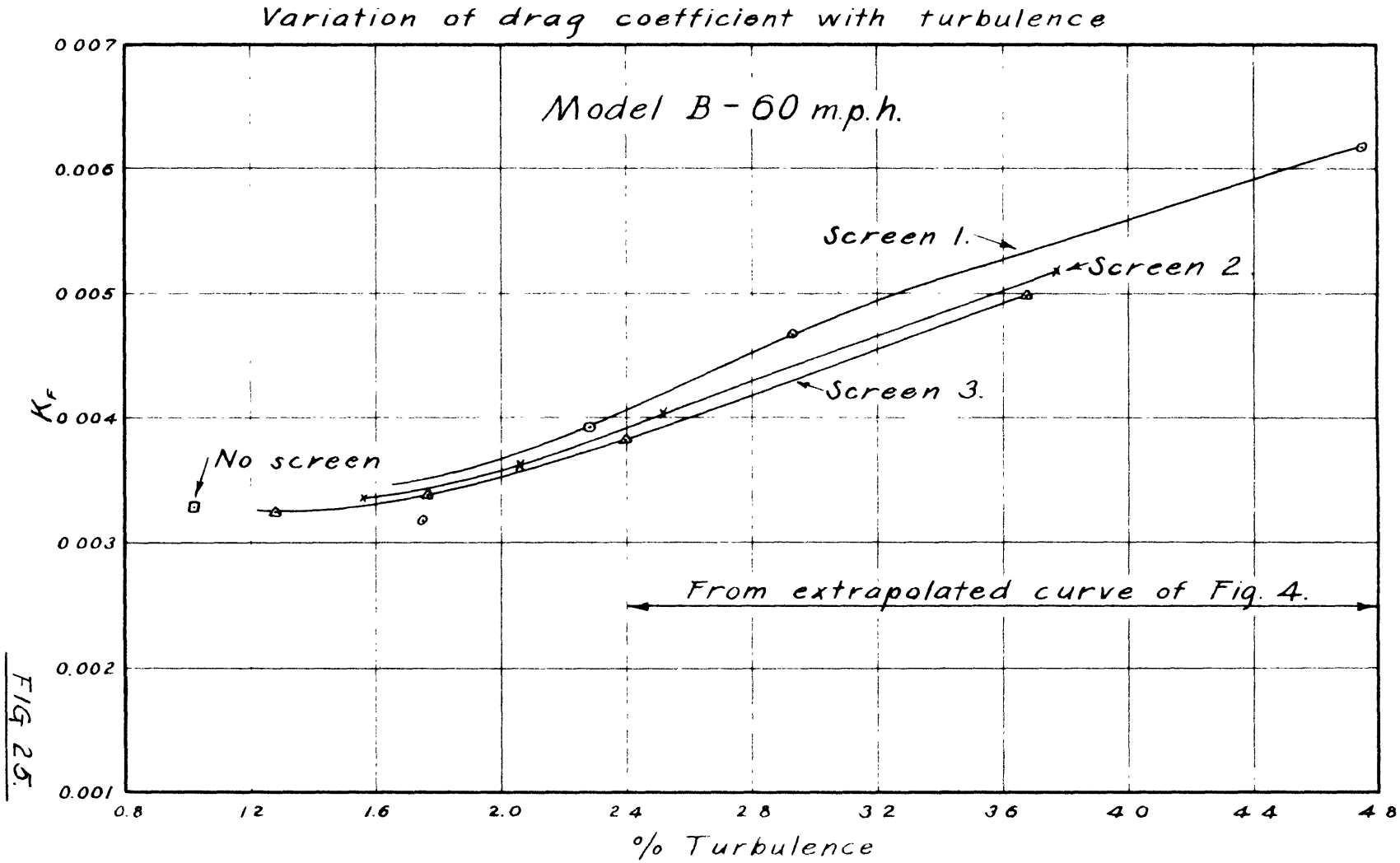
Variation of drag coefficient with turbulence
Model B - 60 m.p.h.
Screen 1.
Screen 2.
Screen 3.
No screen
From extrapolated curve of Fig. 4.
K_F
0.007
0.006
0.005
0.004
0.003
0.002
0.001
0.8
1.2
1.6
2.0
2.4
2.8
3.2
3.6
4.0
4.4
4.8
% Turbulence

FIG 25.